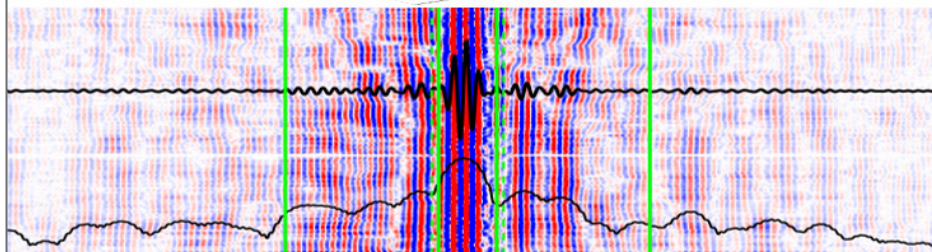
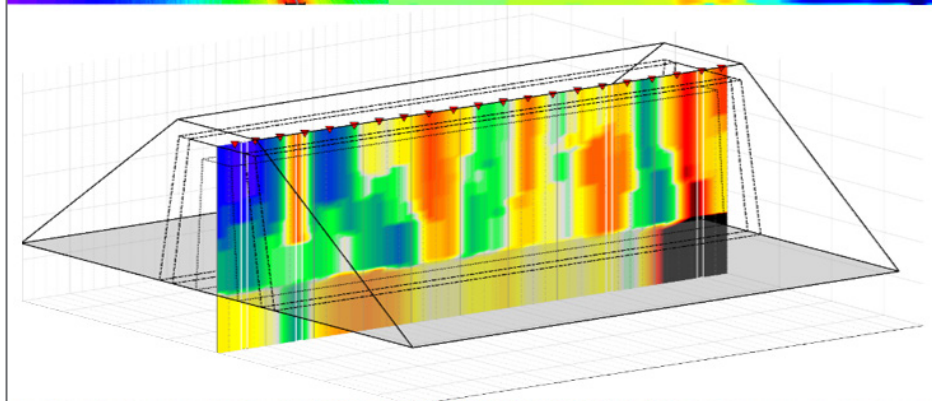
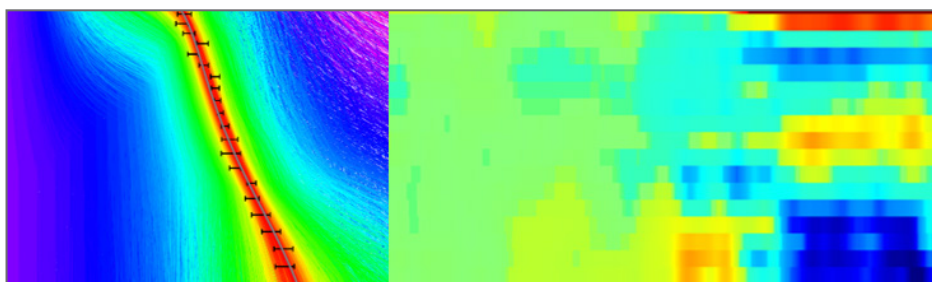
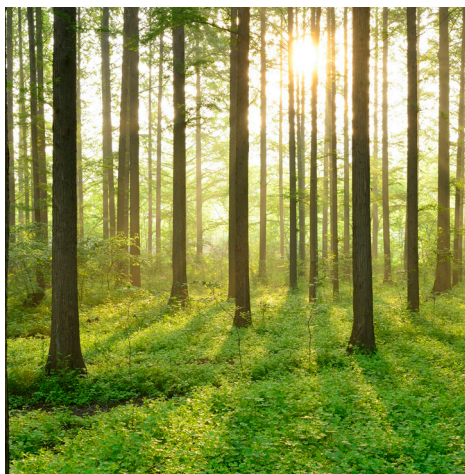


# DISTRIBUTED ACOUSTIC SENSING FOR DETECTION OF DEFECTS IN THE TEST DAM AT ÄLVKARLEBY

REPORT 2021:732





# **Distributed Acoustic Sensing for Detection of Defects in the Test Dam at Älvkarleby**

**SAM JOHANSSON  
SOPHIE BEAUPRETRE  
ANAÏS BOUE  
ANNA STORK**

ISBN 978-91-7673-732-3 | © Energiforsk mars 2021

Energiforsk AB | Phone: 08-677 25 30 | E-mail: [kontakt@energiforsk.se](mailto:kontakt@energiforsk.se) | [www.energiforsk.se](http://www.energiforsk.se)



## Foreword

**The project builds on the project *Fibre-Optic Distributed Acoustic Sensing for Detection of Seepage and Internal Erosion* (Energiforsk report 2020:682). Acoustic measurements were performed in the test dam at Älvkarleby with the aim to assess the capabilities of Ambient Noise Interferometry (ANI) with DAS data to monitor earthen dams. The analysis indicates that available ANI methods can be applied at small-scale dams to image and monitor the infrastructure using fibre-optic DAS data.**

The work has been performed by HydroResearch (Sam Johansson, project leader), Silixa (Anna Stork) and Sisprobe (Sophie Beaupretre and Anais Boue). The work has been followed by a reference group consisting of Henrik Arver, Swedish Regulation Enterprises, Christian Bernstone, Vattenfall, Kerim Genel-Waldenström, Vattenfall, Sezar Moustafa, Fortum, and Petter Westerberg, Uniper.

The project has been carried out in the framework of the Energiforsk Dam Safety R&D Program with participation from the Swedish hydropower industry and Svenska kraftnät. The authors are responsible for the content.

## Sammanfattning

Optiska fibrer för distribuerad mätning finns installerade i nästan 100 dammar i Sverige idag. Dessa används för detektion av läckage baserat på distribuerad temperaturmätning (Distributed Temperature Sensing, DTS) eller detektion av rörelse baserat på distribuerad töjningsmätning (Distributed Strain Sensing, DSS). Flertalet installationer kan numera även användas för distribuerad akustisk mätning (Distributed Acoustic Sensing, DAS). Detta är en metod som är under snabb utveckling både beträffande mät- och utvärderingsteknik. Med metoden kan förändringar av dammens materialegenskaper upptäckas, dvs. områden där förändringar skett kan upptäckas (exempelvis lägre packningsgrad, högre vattenhalt, svaghetszoner, inre erosion). Förändringarna kan följas i tiden genom kontinuerliga mätningar, vilket gjorts i detta projekt.

Projektets syfte var att testa och utvärdera tekniker som baseras på analys av omgivande brus (Ambient Noise Interferometry, ANI). Mätningarna gjordes i den 20 m långa experimentbyggnadsdamm som byggts i Älvkarleby. Mätningar gjordes 2020-04-06–2020-06-24, vilket var både före och under uppfyllnad av magasinet. I dammen finns inbyggda, och för projektet ej kända svagheter, vilka kommer att presenteras av dammägaren under 2021.

Syftet med de analyser som gjordes var främst att:

- analysera hastighetsförändringar som uppkommer vid olika vattenstånd,
- utföra mätningar med en måtenhet (DAS) med bättre upplösning än vad som använts tidigare, samt att
- utvärdera om nuvarande utvärderingsteknik baserad på ANI kan användas även i denna lilla skala.

Utvärdering utfördes av såväl materialegenskaper i rummet vid en given tidpunkt (imaging), som av förändringar under en given tidsperiod (monitoring). Av den förstnämnda metodiken framkom flera avvikande områden med högre eller lägre hastigheter än medelvärdet. Genom användning av den andra metoden kunde hastighetsförändringar upptäckas, vilka ändras när vattennivån i magasinet samt vattenhalten i jordmaterialet ändras. Dessa förändringar varierade längs dammen, samt på olika nivåer i dammen. Som exempel kan nämnas en hastighetsminskning mellan sek 0 och sek 6 m, vilken framkommer vid hög vattennivå. Detta indikerar ett område med hög vattenmättnad.

Sammanfattningsvis indikerar de båda ANI baserade analysmetoderna att dessa även kan tillämpas i denna skala för utvärdering av materialegenskaper, samt för att följa eventuella förändringar. Detta innebär att fiberbaserad mätmetodik kan utvecklas vidare. Utvärderingen kan också förbättras genom att även inkludera effekter av yttre faktorer som nederbörd, vilket inte varit aktuellt i dessa mätningar.

Nyckelord: Distribuerad akustisk mätning, Inre erosion, Fyllningsdammar.

## Summary

Optical fibres are installed in almost 100 dams in Sweden today. They are used for detection of seepage (based on Distributed Temperature Sensing, DTS) or movement (based on Distributed Temperature and Strain Sensing, DTSS). Most of those installations can also be used for acoustic measurements (Distributed Acoustic Sensing, DAS). The recent development of the technology, regarding both monitoring and analysis techniques, may give an additional method to study the seepage/internal erosion phenomena in dams and furthermore to provide information on the integrity. This possibility is investigated further in this study.

The aim of this study was to assess the capabilities of Ambient Noise Interferometry (ANI) with DAS data to monitor earthen dams. The monitoring was conducted at the recently constructed 20 m-long Test Dam at Älvkarleby with continuous DAS data recordings 6 April to 24 June 2020. Defects have been incorporated in this dam and the aim is to determine the location of these defects. The reservoir behind the dam was filled over the monitoring period.

The objectives of the analysis were to:

- Perform measurements during reservoir filling to detect changes in material properties.
- Perform measurements using a DAS unit with 3m gauge length to improve the spatial resolution compared to previous measurements.
- Determine whether available ANI methodology can be applied at such small-scale dams to image and monitor the infrastructure.

Both ambient noise imaging and monitoring are carried out. The imaging results highlight several areas in the dam that could be caused by inhomogeneities or defects. The monitoring analysis reveals a clear anti-correlation of the velocity variations and water filling, suggesting a sensitivity of the seismic waves to water content in and/or around the dam. Different sections of the dam respond differently to the increase in water level. For example, a decrease in seismic velocities between 0m and 6m dam chainage when the water level is high could indicate a weak point in the dam at this point with an increase in water saturation.

Overall, the analysis indicates that available ANI methods can be applied at small-scale dams to image and monitor the infrastructure using fibre-optic DAS data. With additional information further analysis of the data could separate environmental from hydrogeological effects.

Keywords: DAS, Distributed Acoustic Sensing, Internal erosion, Embankment dams.

## List of content

<b>1</b>	<b>Introduction</b>	<b>7</b>
<b>2</b>	<b>Objective</b>	<b>8</b>
<b>3</b>	<b>Monitoring requirements</b>	<b>9</b>
	3.1 Overview	9
	3.2 Seismic methods	9
<b>4</b>	<b>Distributed Acoustic Sensing (DAS) monitoring technology</b>	<b>11</b>
<b>5</b>	<b>Cable installation and measurements</b>	<b>13</b>
	5.1 Background	13
	5.2 The Älvkarleby TEST dam	13
	5.3 Cable installations	15
	5.4 DAS Monitoring Set-Up	15
	5.5 Measurements	17
<b>6</b>	<b>Monitoring and imaging methods</b>	<b>19</b>
	6.1 Introduction	19
	6.2 Ambient Noise Interferometry (ANI)	19
	6.3 ANI DAS measurements	21
	6.4 ANI imaging methodology	21
	6.5 Inter-cable cross-correlations for imaging & monitoring	24
	6.6 ANI monitoring methodology	25
	6.7 Active seismic survey data	27
<b>7</b>	<b>Results</b>	<b>30</b>
	7.1 Imaging using crest cable	30
	7.2 Preliminary inter-cable imaging results	33
	7.3 Monitoring	34
	7.4 Summary and Discussion	37
<b>8</b>	<b>Conclusions and Recommendations</b>	<b>39</b>
	8.1 Conclusions	39
	8.2 Extension of the analysis	40
<b>9</b>	<b>References</b>	<b>41</b>

# 1 Introduction

The use of optical fibres for dam monitoring started in 1998. The technology is widely used in existing embankment dams and is almost a standard in new dams in Sweden today. The most common application is seepage flow monitoring based on temperature measurement, but also strain measurements are used. Initial tests have also been made using Distributed Acoustic Sensing, DAS (Johansson et al., 2020).

The recent development of the DAS technology, regarding both monitoring and analysis techniques, may give an additional method to study the seepage/internal erosion phenomena in the dams. The application of this monitoring technology will be easy to apply especially in dams where fibres are already installed.

Vattenfall has, in accordance with the Swedish dam safety guideline (Swedenergy 2017), designed and built an experimental embankment dam at their laboratory facilities in Älvkarleby. The dam has six built-in defects, that all represent damages that eventually could evolve to a dam break. These defects are sized to be realistic, while still large enough to be realistically detected in blind-tests by suitable geophysical methods. The investigations/monitoring began in Spring 2020 and will continue until Summer/Autumn 2021. The location and size of the defects will be revealed at the end of 2021, after the investigators have presented their reports. Several methods will be applied by different institutions and companies both for short time measurements (in terms of campaigns) and long-term measurement. Fibre optic cables are installed for measurement of temperature, strain, and acoustic signals.

This report describes the acoustic measurements carried out during the first filling of the dam reservoir for the test dam. The work on site was performed by Carl Nygren and Sam Johansson, HydroResearch. Measurements were set-up remotely by Anna Stork and Ariana David at Silixa. The final data analyses were made by Aurélien Mordret, Sophie Beauprêtre, Anaïs Lavoué and Roméo Courbis, Sisprobe, using the Ambient Noise Interferometry (ANI) approach (Curtis, et al. 2006).

## 2 Objective

Existing methods can detect seepage changes close to the measuring point. Sometimes this is good enough, but there is also sometimes a need to obtain information from a larger area. This can be achieved using DAS because it has the ability to detect material changes far away from the fibre optic cable and identify events that can create seepage flow changes. Both passive and active measurement techniques could be used.

The test dam offers a possibility to test the capability of DAS to detect such changes on a small scale. The small size of the dam poses challenges for DAS to detect the built-in, and for us un-known, defects. For example, higher frequency seismic wave analysis is required than has previously been tested.

The objective of these tests was to:

- Perform long-term measurements during reservoir filling to detect changes in the material properties of the dam.
- Perform measurements with a DAS interrogator with a 3m gauge length to improve the spatial resolution compared to previous measurements. This should in some way compensate for the small size of the dam.
- Determine whether available ANI methodology can be applied at such small-scale dams to image and monitor the infrastructure.

Greater imaging and monitoring possibilities available compared to the earlier DAS monitoring results from Näs because fibre optic cables are installed throughout the dam, this could allow a 3D picture of the dam to be built.

## 3 Monitoring requirements

### 3.1 OVERVIEW

Internal erosion is the reason for almost 50% of the failures of embankment dams (Foster et al. 2000; Fell et al. 2005) and a large body of research has been performed to understand, detect, and prevent this mechanism (ICOLD 2015).

In the case of internal erosion, there is an expected change in leakage flow, porosity, and water saturation (due to higher water level/pressure). To detect damage in dams, any suitable method must be able to measure deviations in those parameters either directly or in a secondary parameter caused by changes in the primary parameters.

Previous studies have shown that methods that record parameters related to leakage flow or changes in leakage flow, such as temperature, are more sensitive than those that record material properties/material changes (Johansson, 1997; Sjö Dahl, et al. 2019). Most methods, however, measure indirect/secondary parameters, which are further interpreted for a dam safety assessment. These methods include seismic methods

### 3.2 SEISMIC METHODS

Small change in material properties may be detected with accurate and precise seismic monitoring. On the other hand, the sensitivity of seismic methods in space is limited by the frequencies, and hence wavelengths, analysed. If an anomaly is smaller than approximately  $\frac{1}{4}$  wavelength in extent it will not be resolved because passage of the wave will be undisturbed by the anomaly.

The sensitivity of seismic methods in time is limited by the changes in seismic properties due to changes in a dam. The internal erosion of sediment in a dam or seepage through a dam result in changes in the material properties. The effect of these properties on compressional (P- wave) and shear wave (S-wave) seismic velocities,  $V_P$  and  $V_S$  respectively, is given by the following equations:

$$V_P = \sqrt{\frac{K + \frac{4}{3}\mu}{\rho}} \text{ (Eqn. 1) and}$$

$$V_S = \sqrt{\frac{\mu}{\rho}} \text{ (Eqn. 2)}$$

where  $K$  is the bulk modulus,  $\mu$  is the shear modulus and  $\rho$  is the density.

Therefore, an increase in water saturation, for example due to water level rise or precipitation/ snow melt, generally results in a decrease in S-wave velocity and an increase in P-wave velocity. This is because an increase in  $K$  with water saturation is predicted by the Biot-Gassmann fluid substitution theory (Gassman, 1951; Biot, 1956) and density increases if air is replaced by water.

Material properties could vary not only due to leakage or erosion, but also due to other factors such as climate, compaction or load effects. An increase in load on the dam, for example with a rise in water levels, increases seismic velocities.

Further investigations can be conducted by recording acoustic emissions, produced at high flow rates/flow velocities. These can be measured using seismic instruments or DAS technology.

More noise is generated if fines are transported by the seepage water flow. Research regarding this approach has been performed by Koerner et al. (1976, 1979 and 1981), Buck & Watters (1986), Hung et al. (2009) and Boleve et al. (2012). Additionally, seismic events in fractured bedrock, a concern for dam stability, can be recorded by seismic instruments and DAS.

## 4 Distributed Acoustic Sensing (DAS) monitoring technology

DAS technology has undergone significant development and improvements in the last decade. The technique can be used to effectively measure the speed of sound and seismic waves in soils, rocks and fluids in many different scenarios. Like Distributed Temperature Sensing (DTS), DAS only requires an interrogator unit, a power source and a fibre optic cable to measure dynamic strain (Parker et al., 2014). DAS technology has been deployed for borehole monitoring, ground movement detection, and pipeline monitoring in many industries, such as oil and gas, geothermal exploration and CO<sub>2</sub> sequestration, and in remote and harsh environments (e.g., Becker et al., 2019; Jousset et al., 2018; Nikles 2009).

DAS measurements are made on fibre-optic cables which may be the same fibre-optic cables installed for temperature sensing. A DAS system provides a sensor array that is unmatched in spatial resolution and sampling capabilities by traditional seismic instruments, while allowing the application of processing methods developed for use with traditional seismic arrays (Lindsey, et al. 2017). The propagation of the acoustic energy in the ground can be analysed in to determine the speed of sound and assess the ground composition.

The operating principle for DAS is illustrated in Figure 1. A pulse of light is emitted from the DAS interrogator and travels down an optical fibre. Measurements can be made on fibres up to tens of km long and a single-mode or multimode cable can be used with the system. A small amount of the light is naturally scattered in the fibre and returns to the interrogator unit. An optoelectronics architecture in the sensing unit measures the amplitude and phase of the backscattered light. When an acoustic or seismic wave exerts tiny pressure/strain changes on the fibre this changes the amplitude and phase of the backscattered light. The relative phase and amplitude can be used to determine the strain rate on the fibre.

The sensing system measures changes in strain at a rate of up to several tens of kHz, required to accurately record acoustic fields. The system digitally records the response at evenly spaced measurement points or channels along the fibre. The Silixa intelligent DAS (iDAS™) system (Figure 1) can offer spatial sampling of 1-m with a dynamic range of more than 120 decibels and with no cross-talk between adjacent measurements. The spatial resolution, or gauge length, of the system can be tuned to the individual application. Standard gauge lengths are 3 m and 10 m. Short gauge lengths improve the spatial resolution but results in a lower signal-to-noise ratio (SNR).

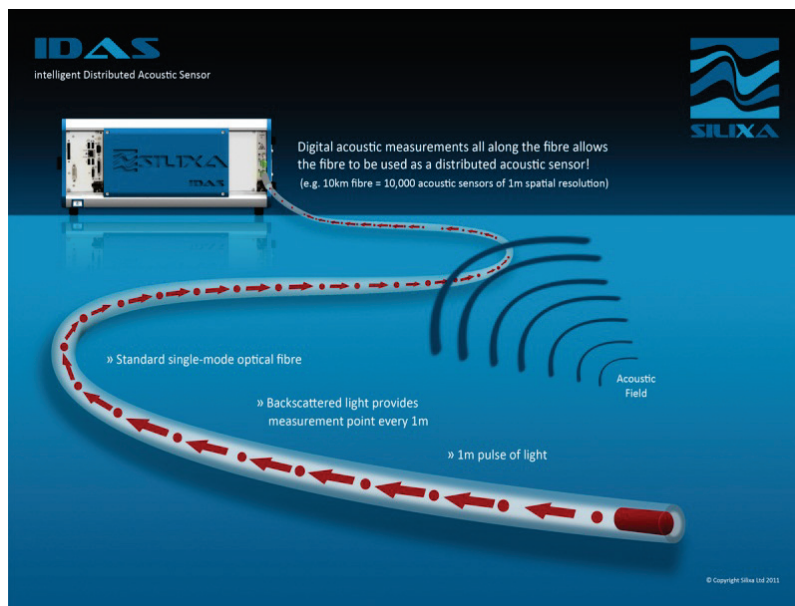


**Figure 1** The iDAS™ provides digital acoustic measurements along the entire length of single-mode fibre. The interrogator emits pulses of laser light along the fibre and measures the phase and amplitude of the backscattered light from every measurement point (channel) along the fibre.

The use of DAS for seismic surveys has been validated through the use of traditional seismic processing methods to compare DAS results with those from traditional seismic surveys and laboratory testing (e.g., Jousset et al., 2018; Lindsey et al., 2017; Parker et al., 2014).

## 5 Cable installation and measurements

### 5.1 BACKGROUND

The design of the test dam was based on experiences of a previous blind test in Norway in 2003 where the potential of resistivity, self-potential and temperature surveying was undertaken on a rockfill embankment dam (Johansson, 2005). The dam, with a height of 5.25 m and a length of 37 m, was built with a central core of moraine with supporting rock fill and with in-built defects. It was known from a desktop sensitivity study based on the material properties of the building materials that it would not be possible to detect small defects using single campaign surveys. However, geophysicists managed to indicate defect locations by testing a monitoring approach investigating changes over time. The Norwegian blind-test dam was not built as a conventional earth embankment dam, where there would normally be filters separating the impermeable core from the outer coarse pervious shell (rock fill). The experimental dam at Älvkarleby, was however designed in accordance with the Swedish dam safety guidelines.

### 5.2 THE ÄLVKARLEBY TEST DAM

The chosen embankment dam design is a 20-meter-long dam where the impermeable core is supported by two connecting filter zones and support fills (Figure 2). The height is 4 meters, and its base against the foundation perpendicular to the dam line is 15 meters. The two sidewalls which the dam connects to are slightly angular (12,5 %). The bottom slab is inclined 1% towards the downstream side, where a ditch collects the seepage water through the dam body. This seepage is divided by ribs into eight sections which are continuously monitored by flow. However, the result will be revealed in the end of the experimental dam project.

The dam rests on a rigid concrete support structure submerged into a riverbank of 12 meters of sand overlying bedrock (drained conditions). The experimental dam thus has its crest in line with the surrounding ground. To the extent possible, the design is made to avoid structural members with negative impact on geophysical measurements. The bottom concrete slab of the containment has therefore been reinforced with fibreglass reinforcement bars. Since there is no electrically conductive reinforcement this resembles foundation on rock.

From an acoustic point of view the surrounding concrete walls will create seismic wave reflections which will complicate the evaluation.



Figure 2 Pictures of the crest and downstream face and upstream face of the test dam before filling.

The built-in defects, that all represents damages that eventually could evolve to a dam break, are:

1. Cavity in the core (wood cube  $0.4 \text{ m} \times 0.4 \text{ m} \times 0.4 \text{ m}$ ).
2. Horizontal permeable zone passing through the core (rectangular cross section  $0.1 \text{ m}$  high and  $0.5 \text{ m}$  wide).
3. Vertically loose zone (elongated zone with square cross section with side  $0.3 \text{ m}$ ).
4. Lump of concrete or large stone (cube  $0.5 \text{ m} \times 0.5 \text{ m} \times 0.5 \text{ m}$ ).
5. Permeable horizontal zone at side ( $0.1 \text{ m} \times 0.1 \text{ m}$ ).
6. Filter defect on the upstream side.

Being a blind-test, the position of these defects is not known to the investigators (in fact kept secret to a few persons only). They will be revealed later.

### 5.3 CABLE INSTALLATIONS

The cable installation (as showed in Figure 3) is extensive compared to typical installation in large dams, where normally just one or a few cables are installed along the dam. In the test dam there is one cable, placed at four levels in the upstream filter, and on the core crest. Some parts of this cable are also placed in water, allowing the water temperature to be measured. A second cable was used to measure at five levels in the downstream filter, and a third cable is placed closed to the dam toe.

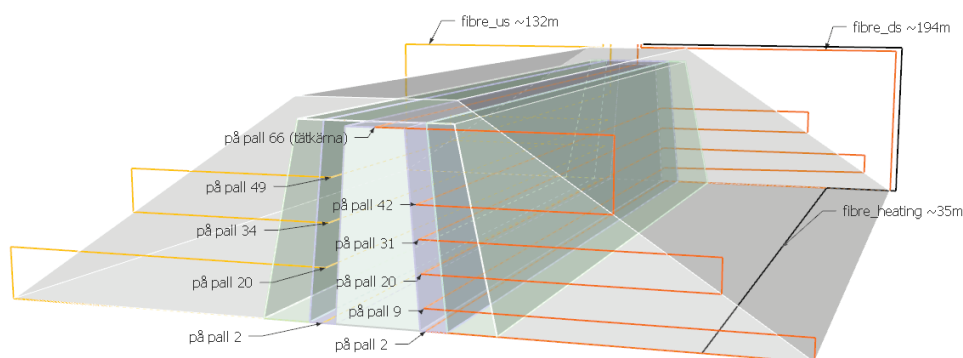


**Figure 3** Cross section of the dam showing the three installed cables.

All cables contain both multimode and single mode fibres. This enables DTS, DAS and Distributed Strain Sensing (DSS) measurement. Furthermore, the cable in the downstream toe contains a copper wire, which can be used for heating for the Heat-Pulse test (“Active DTS method”).

The dam chainage (CH) along the dam starts on top of the dam at the connection to the sloping concrete wall at the left side (CH 0m) and ends at the right abutment at CH 20.6m on the crest. The bottom starts at CH 0.3m and ends at CH 20.3. All data is presented along the dam using dam chainage.

### 5.4 DAS MONITORING SET-UP

An iDAS with a 3 m gauge length was used in this study. This increases noise levels in the data compared to a 10 m gauge length but, given the small horizontal extent of the dam (20 m), the unit with the smaller spatial resolution (3 m) was required. The equipment was installed at site by HydroResearch (Figure 4) and the set-up of the iDAS was performed remotely by Silixa using the parameters given in Table 1. To assess data quality the noise levels were verified to be as expected (Figure 5) and calibration “tap tests” were performed on the cable to calibrate channel positions in the dam (Figure 6).



Figure 4 Monitoring unit for DAS and DTS, inside the monitoring container.

Table 1 iDAS parameters used in data acquisition.

Parameter	Value
Gauge length	3 m
Sampling frequency	1000 Hz
Spatial sampling	0.5 m

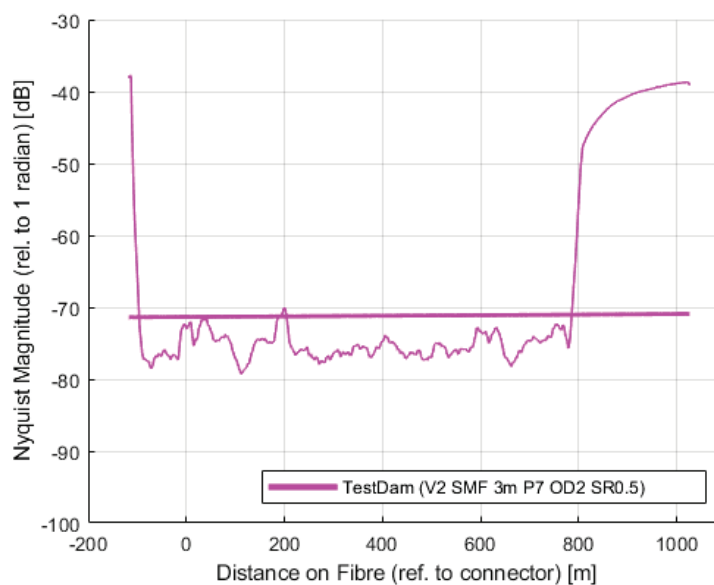


Figure 5 Theoretical noise floor for the Test Dam iDAS set-up (thick line) and the measured noise level along the cable (thin line).

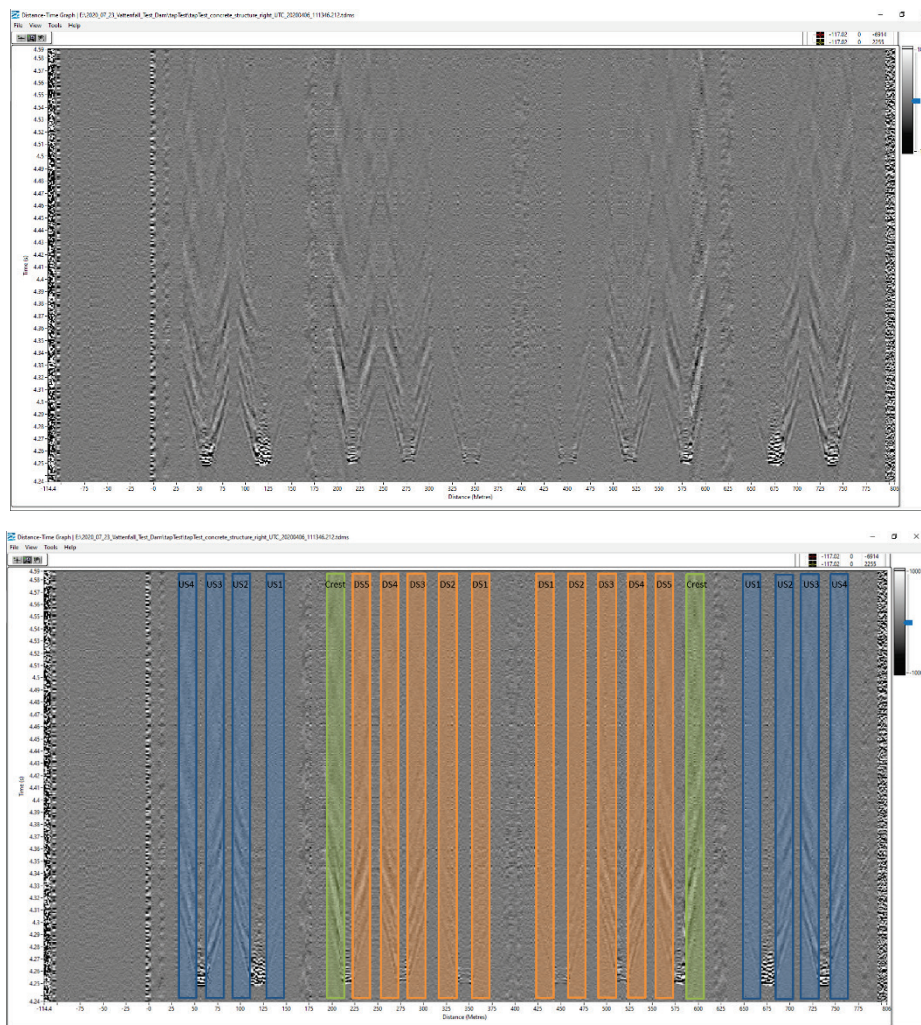
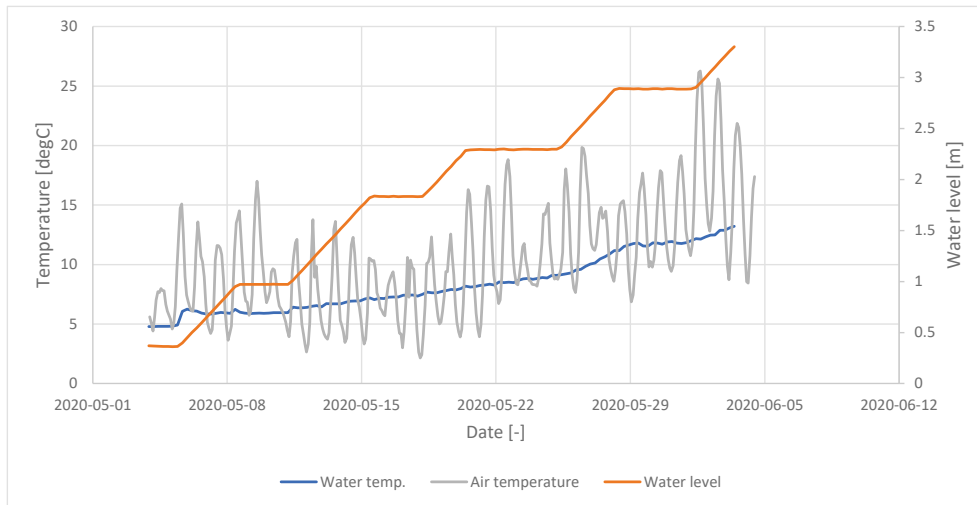


Figure 6 Recording of a tap test at the right hand side of the dam (above). This helps determine the recording channel locations in the dam (below).

## 5.5 MEASUREMENTS

Initial filling of the water started in April but had to be aborted. The main filling of the dam up to the retention water level started on 4 May and was, due to onloading concerns, performed slowly during working days. At weekends, the water level was kept constant. Continuous measurements of the reservoir and air temperatures were made (Figure 7). DAS measurement started on 6 April 2020, i.e., about one month before the filling, and lasted until 24 June 2020.

On 9 and 10 June an active seismic survey was conducted by Uppsala University using both a P- and S-wave source recorded on hydrophones. The locations and approximate timings of these shots were provided to Silixa. The P-wave shots were made on the upstream side of the dam and the S-wave shots were positioned in shallow boreholes in the dam.



**Figure 7 Water levels, and temperature in air and water during filling.**

## 6 Monitoring and imaging methods

### 6.1 INTRODUCTION

Seismic methods can be split into two categories, active and passive. Active seismic methods require a source to produce seismic waves. This source can be produced by, for example, dynamite, a vibroseis truck or a weight drop. The more energetic active seismic sources (e.g., dynamite or vibroseis) are not suitable for use on a dam because they may damage the infrastructure. Passive seismic methods make use of the natural or anthropogenic noise. This can include the recording of natural tectonic events or recording of the ambient noise field. These passive methods do not require direct human intervention, resulting in cost savings compared to active methods. Data can be recorded on-demand, independent of weather conditions or time of day, and can be performed continuously if required. All seismic methods make use of seismic wave measurements created by an active or passive source. The recorded signal provides information on the velocity and amplitude of the waves in the dam and these can then be related to material properties.

Given the advantages of passive seismic methods, this study tests the feasibility of using ANI in combination with DAS measurements to image and monitor changes in the dam. An active seismic survey was conducted by Uppsala University in June 2020 and these shots are recorded by the DAS interrogator. We make an initial assessment of the recordings to determine whether further processing for a reflection, refraction or Multichannel Analysis of Surface Waves (MASW) survey may provide useful information.

### 6.2 AMBIENT NOISE INTERFEROMETRY (ANI)

ANI makes use of naturally occurring and anthropogenic background noise to calculate seismic velocities and hence image the subsurface. By cross-correlating noise records between two sensors, it is possible to reconstruct the Earth's response as if one sensor were a seismic source and the other a receiver. Thus, a seismogram is produced. Since ambient seismic noise travels through the subsurface the same way that active source energy does, it is possible to extract some of the same information that could be gathered from an active survey. The theory of the method is set out in early papers, e.g., Campillo (2006); Wapenaar and Fokkema (2006).

The output from ANI are estimates of seismic wave velocities in the dam/subsurface, with the resolution and depth of investigation dependent on the type of waves investigated and the available frequency bands. Seismic velocities give information on the characteristics of material in the dam/subsurface. For the case of surface waves, lower frequency studies provide information on deeper structures. Additionally, by studying seismic velocity changes through time, it may be possible to detect changes in water saturation or structure.

Different parts of the seismic wavefield can be used for ANI, i.e., body waves, surface waves, and coda waves (see Figure 8). Travelling through the interior of the dam, body waves (P- and S-waves) are direct arrivals and P-waves arrive first

in the virtual seismograms. Surface waves travel slower, tend to be lower in frequency and travel along the surface of the dam. High frequency surface waves sample only the very shallow depths, with lower frequencies penetrating deeper. Surface waves are dispersive, meaning that their phase velocity depends on frequency. Additionally, as seismic waves travel through the subsurface some energy is scattered by inhomogeneities. These randomly scattered waves that arrive later than body or surface waves are known as coda waves. The later in the coda we look, the more scattered the waves are and, for a noise cross-correlation, that means that waves in the coda of the correlation have stayed in the medium between and around the two stations used for the correlation much longer than the direct waves. Coda waves are therefore more sensitive to changes in the medium than direct waves and tend to be more stable with a varying noise sources than body or surface waves. As a result, coda waves are often used in monitoring or time-lapse surveys to improve repeatability when using a permanent array of sensors.

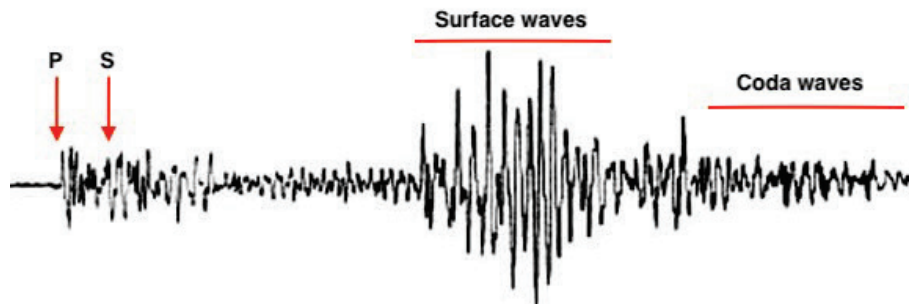


Figure 8 An example seismogram with arrival times and seismic phase names indicated. P- and S-waves are body waves.

Ambient seismic noise is continuous and therefore can be used to continually monitor the subsurface. Ideally the noise field measured should consist of evenly distributed noise sources completely surrounding the measurement area. For stable cross-correlated waveforms, ANI requires noise sources to be unchanging through time.

ANI has been successfully used in the academic community and the oil and gas industry to image the subsurface at different depths and different scales (e.g., Shapiro et al., 2005; Lin et al., 2007). In oil and gas reservoirs the technique can provide information on fluid movement and compaction effects (e.g., de Ridder et al., 2014). In volcanic settings it can aid hazard assessment by tracking velocity changes in the system caused by volcanic gas or magma movement (e.g., Huang et al., 2018). To a limited extent ANI has also been applied to dam structures and landslide sites (e.g., Olivier et al., 2017; Planès et al., 2016; Johansson et al., 2020). These studies have been able to identify changes in the subsurface at the sites. However, the completeness of the imaging has been limited by the use of a small number of point sensors, i.e., geophones. With a dense seismic array, as provided by DAS monitoring, it is possible to conduct a detailed survey of dam and landslide sites. A brief description of the ANI methods used in this survey in Section 6.4.

### 6.3 ANI DAS MEASUREMENTS

The development of capabilities to use ANI with DAS data has significant advantages over traditional methods which use expensive active source seismic surveys and point sensors which require significant manpower to deploy for a large survey. ANI is a passive technique which means the instrumentation is left to record for a given amount of time without needing personnel present. Fibres can be permanently deployed so data can be collected continuously or as required. The distributed nature of DAS recordings and the potential DAS provides to use cables up to 40 km-long means that information is available over large distances and down to sub-metre scales, if required.

### 6.4 ANI IMAGING METHODOLOGY

Once cross-correlations between each station pair are obtained, the processing steps are similar to those conducted for MASW surveys to obtain a velocity versus depth profile. There are three main steps: i) phase velocity dispersion curve measurements; ii) travel-time tomography, Eikonal tomography in this study; iii) depth inversion.

Eikonal tomography is based on the Eikonal equation stating that the local slowness  $s_{ij}$  is related to the spatial gradient of the wave travel-time  $t_i$  from virtual source  $i$  to the location  $x_j$  as:

$$s_{ij} = \nabla t_i(x_j) \quad (\text{Eqn. 3})$$

For a 1D geometry,  $s_{ij} = \nabla t_i(x_j)$  (Eqn. 3) simplifies to:

$$s(x) = \frac{1}{N} \sum_{i=1}^N \frac{\partial t_i(x)}{\partial x_i} \quad (\text{Eqn. 4}),$$

where  $s$  is the local phase slowness,  $N$  the number of virtual sources, and  $x_i$  the offset relative to the position of the virtual source. The success of this process relies on an accurate picking of the wave travel-time along the fibre. To do so, positive and negative sides of the cross-correlations are averaged before being sorted in virtual shot gathers (see Figure 9a). The correlations are then bandpass filtered between 15-35 Hz, and windowed, i.e., the amplitudes outside of the window are tapered and muted (black line in Figure 9a). The travel-time of the wave is measured in the frequency-space domain where  $t_i(x) = \frac{\phi(x_i, \omega)}{\omega}$  with  $\phi$  the phase of the correlation,  $\omega$  the angular frequency, and  $x$  the offset. The travel-time curves are interpolated onto a regular spatial grid with a spatial sampling of 0.25 m before smoothing and a gradient computation. To avoid near-source effects, travel-time is measured for offsets larger than one third of the wavelength (see Figure 9b and c). As the travel-time is frequency dependent, which indicates a dispersion phenomenon (see Figure 9a), dispersion can be used to perform a depth inversion of the frequency-dependent velocity to obtain depth-varying shear-wave velocity profiles inside and beneath the dam.

Before computing the gradient of measured travel-times ( $s_{ij} = \nabla t_i(x_j)$ ) (Eqn. 3) smoothing is needed to stabilize the computation (see Figure 9d). Because the final velocity profile is the inverse of the average of

slowness (Eqn. 4) obtained from each virtual source, reliable uncertainties on the velocity can be determined as the standard deviation from the mean of the distribution of velocities.

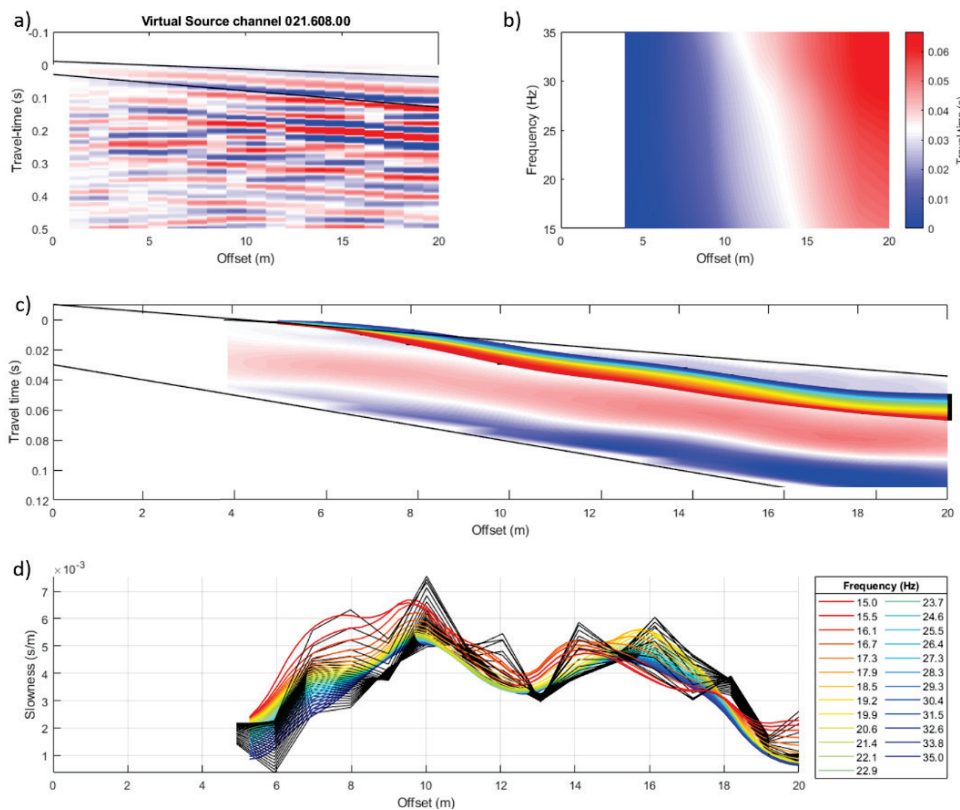


**Figure 9** Example of travel-time picking and eikonal tomography for Channel 608 taken as the virtual source: a) Virtual shot gather bandpass filtered 15 – 35 Hz; b) Fourier transform c) Travel-time measurements superimposed onto muted shot gather d) Coloured lines represent smoothed slowness measurements and black lines raw measurements (i.e., without smoothing).

In the next depth inversion processing step, wave dispersion measurements are assimilated to Rayleigh-type surface waves, although the type of horizontal waves measured along the dam is uncertain. Each point is inverted independently from adjacent points (Figure 10) to form the velocity model (Figure 11). To invert data, we use an algorithm (described in detail in Mordret et al., 2014) based on the Monte-Carlo method. The algorithm conducts a search for the optimal parameters that minimize the difference between the synthetic dispersion curves and the observed curves. At each iteration, the algorithm progressively focuses its search for parameters among the optimal parameters found at the previous iteration.

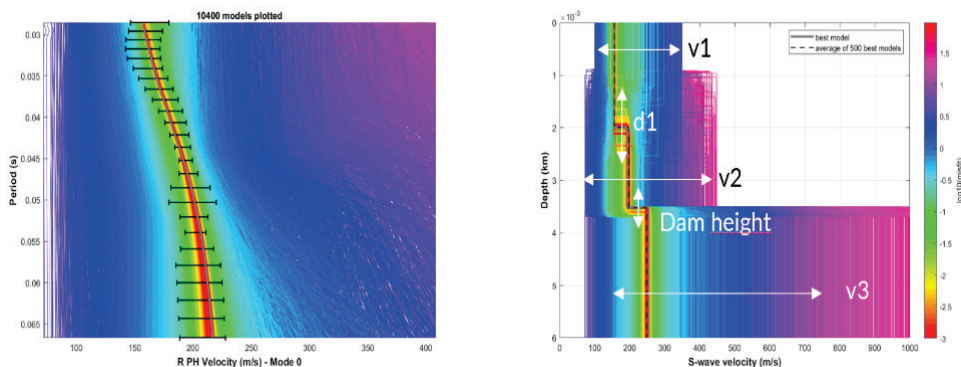


Figure 10 Example of local depth inversion for Point 5 at X=1m. Data is represented by black error bars. Sampled models and associated synthetic dispersion curves are in colour (the colour depends on the misfit value) and the best model is in gray.

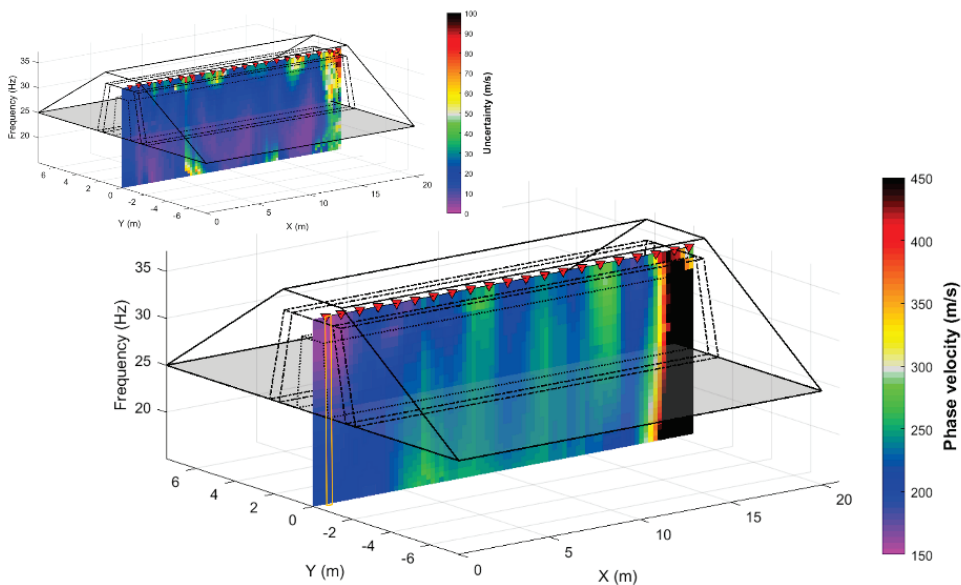


Figure 11 Section of phase velocity measurements together with uncertainty (i.e., standard deviation) section.

The tested model space is defined *a priori* by fixed parameters such as the number of layers and by varying parameters allowed to span a range of values (see Table 2). The selected parameterisation describes a model with 3 layers, including 2 in the dam and 1 below it, and a halfspace. Velocities and thicknesses of these layers are related to each other by simple relations or constrained by *a priori* knowledge such as dam height (see Table 2).

Table 2 Model space parametrization.

Parameter	Description	Min	Max
d1	Dam height	0.25	0.75
delta 1	Uncertainty on dam height	-0.1m	0.1 m
v1	Velocity in the first layer	100	350
v2	Velocity in the 2nd layer * v1	0.7	1.3
v3	Velocity in the third layer * v2	0.85	3.5
vhs	Velocity in the halfspace * v3	0.85	3.5

The inversion algorithm requires a P-wave model ( $V_p$ ) and a density model ( $\rho$ ) to compute the dispersion curves. We used values of  $V_p/V_s$  ratio and density values found in Johansson et al., in prep, ICOLD Congress. Error bars on the dispersion curve picks correspond to the standard deviation in the data (see Figure 10).

5000 models were sampled every 9 iterations. The final velocity model is the average of the 300 best models, i.e., with the lowest misfit. Uncertainty on the final  $V_s$  profile is the standard deviation over these 300 models.

## 6.5 INTER-CABLE CROSS-CORRELATIONS FOR IMAGING & MONITORING

Cross-correlations across the dam were computed between fibre sections USL2 and DSL3 on channels with a 1.5 m spacing. Cross-correlations were stacked to improve Signal to Noise Ratio (SNR). A first insight into lateral velocity variations inside the dam is obtained by computing the correlation coefficient between individual correlation and the average of correlations between facing channels (paths in light green in Figure 12).

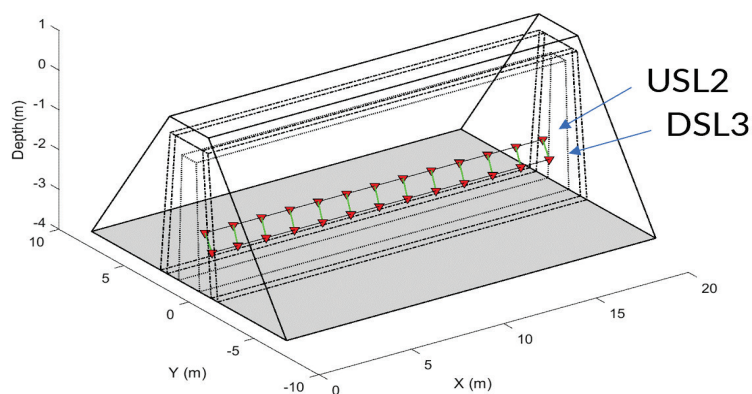


Figure 12 USL2-DSL3 locations in the dam. Red triangles represent channels used to compute inter-fibre correlations. Light green lines represent paths used for computing the correlation coefficient.

## 6.6 ANI MONITORING METHODOLOGY

We use coda-wave interferometry to measure the relative seismic velocity changes within the dam for the whole monitoring period.

Ambient noise monitoring relies on comparing a “Reference” correlation with a “Current” correlation in terms of phase-shift between the two waveforms and the evolution of this phase-shift with the lag-time of the correlations. Here we use a method called coda-wave interferometry (Snieder et al., 2002). For a homogeneous change of the medium (i.e., a homogeneous increase or decrease of the medium velocity,  $\delta v$ ), the time-shift ( $\delta t$ ) in the coda between an unperturbed “Reference” correlation and a perturbed “Current” correlation increases linearly with the lag-time  $t$  along the coda as:

$$\delta v/v = -\delta t/t, \text{ (Eqn. 1)}$$

The monitoring application is performed on 19 channel pairs with similar inter-sensor distances sampled along the dam every 2 m with 1 m overlap, on the crest fibre. Stable results are obtained with a temporal resolution of 30 minutes.

To measure the time shift between a “Reference” and a “Current” correlation, the stretching method of Obermann and Hillers (2019) is applied. Figure 13 illustrates this method. The “Current” correlation is stretched with different velocity variation coefficients and compared to the “Reference” trace. The variation giving the maximum correlation coefficient, giving a measure of the velocity difference between the “Current” and the “Reference” traces. This is adapted when the changes are large and might induce cycle-skipping at large lag-times, as in this case where velocity changes up to 30% are observed in the dam at relatively high frequency, increasing the risk of cycle-skipping issues.

We repeat the procedure for each selected pair of sensors along the dam, but before doing so we carefully select a “Reference”, a frequency band of analysis and a lag time over which the stretching method will be applied.

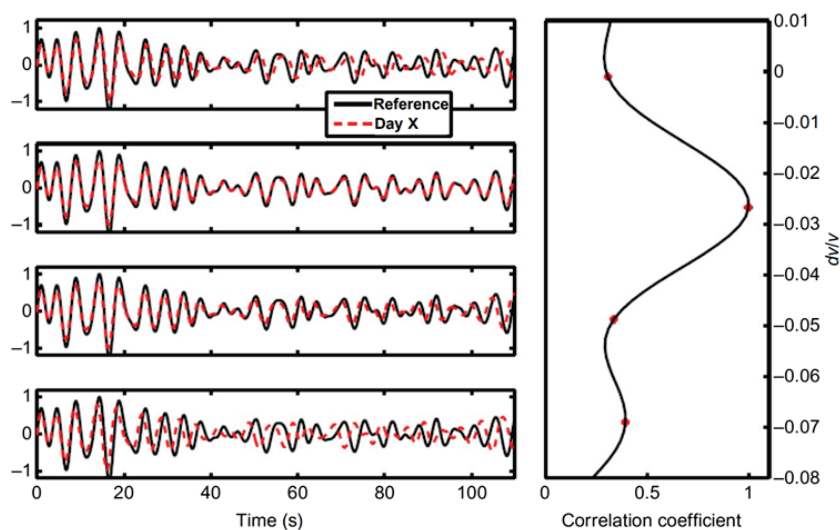
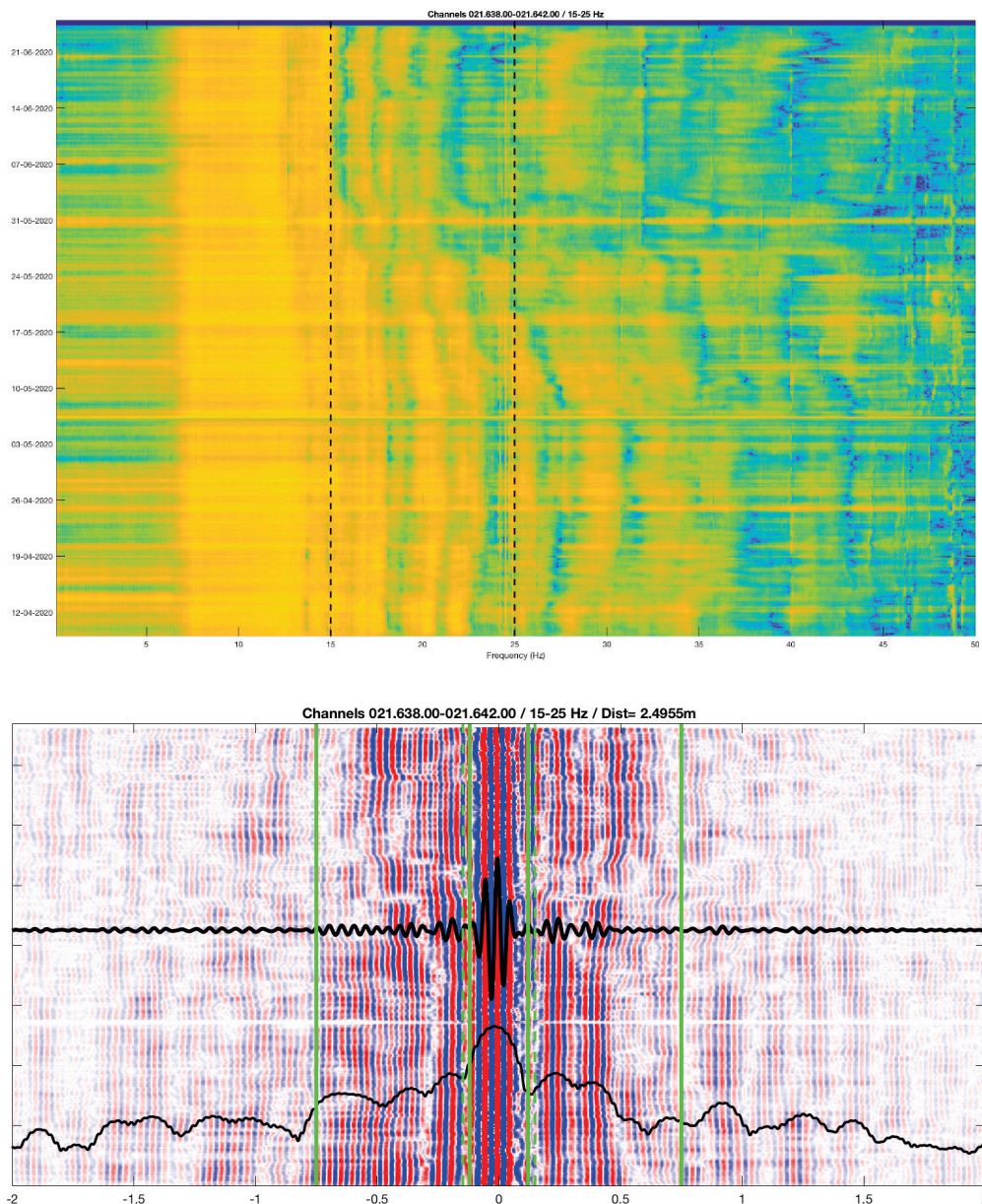


Figure 13 Stretching method. Left: the red signal has been stretched for different values of  $\epsilon$ . Right: the calculated correlation coefficient between the stretched and the reference trace (black) for the different values of  $dv/v$ . From Obermann and Hillers (2019).

The reference correlation should be representative of an average state of the monitored medium. We calculate the mean of all correlations during the most stable period of recording (up to 10 May, Figure 14). The correlation coefficients between the mean correlation and the individual ones are then computed and the final "Reference" is taken as the average of all correlations having a correlation coefficient  $\geq 0.85$  with the mean correlation. This procedure allowed us to reject the correlations that are corrupted and not representative of the medium state.



**Figure 14: Top Spectrogram of correlations from the sensors 021.638-021.642. The frequency band of interest is shown by the black dotted lines. Bottom: Individual 30-min correlations ordered according to the calendar time (y-axis is common with spectrogram). The time bound by the green lines indicates the lag-times used for the monitoring measurements. The black curve at the bottom of the figure shows the logarithm of the envelope of the Reference correlation, used to define the coda windows. The black correlation is the Reference correlation.**

Figure 14a shows the spectrogram of a set of correlations for channel 021.638-021.642, together with the corresponding correlogram (Figure 14b). Velocity variations are clearly observed in the data, from 10 May onwards. These variations are observed from 15 to about 45 Hz. The frequency band will determine the type of wave used for the monitoring and its sensitivity to changes in the medium. For our analysis the frequency has to be high enough so that the wavelength is short enough for the wave to be mostly sensitive to the dam in the surroundings of the two sensors used for the correlation. After trial-and-error, the frequency band 15-25 Hz is found to be the most suitable to measure velocity changes. Above 25 Hz, measurements of velocity variations are difficult because of the noisy nature of the signal.

The time window used determines the type of wave (direct or scattered) used for the monitoring. It also determines the volume sampled by the wave and therefore the spatial resolution of the monitoring results. The later in the coda of the correlation the window is, the longer the wave has stayed in the medium to sample and accumulate its changes. Longer lag-time are more sensitive to changes but scattering and attenuation decrease the amplitude and the quality of the signal. To choose the proper window we balance this trade-off. We use the amplitude of the envelop of the correlation (Figure 14b, in log-scale) to determine the coda window of interest: due to scattering and diffusion, the (log-scaled) amplitude of the envelop should decrease linearly and reach a low background amplitude when the noise level is reached. The coda windows are chosen to be symmetrical around the zero lag-time, along the linearly decreasing coda envelop. After trial-and-error, the window 0.15-0.75 s on both side of the correlations is chosen.

## 6.7 ACTIVE SEISMIC SURVEY DATA

For the analysis of the active seismic data, the timings of the shots were provided by Uppsala University to the nearest second. Recordings of the shots are extracted from the continuous data according to these times to assess the quality of the recordings and timing accuracy.

With good quality DAS recordings, it is possible to conduct a range of seismic surveys including refraction, reflection or MASW (Multi-channel Analysis of Surface Waves). Most shots are well-recorded along the full length of the fibre, for example see Figure 15. The information provided stated the shot times were 10 ms after the second given. However, the shots arrive too late for this to be the case as travel-times within the dam are expected to be about 10 ms or less (see Figure 15). Uppsala University were unable to provide more accurate timings and therefore significant further work would be required to analyse the active shot data. We therefore provide a brief summary below of some observations in the data.

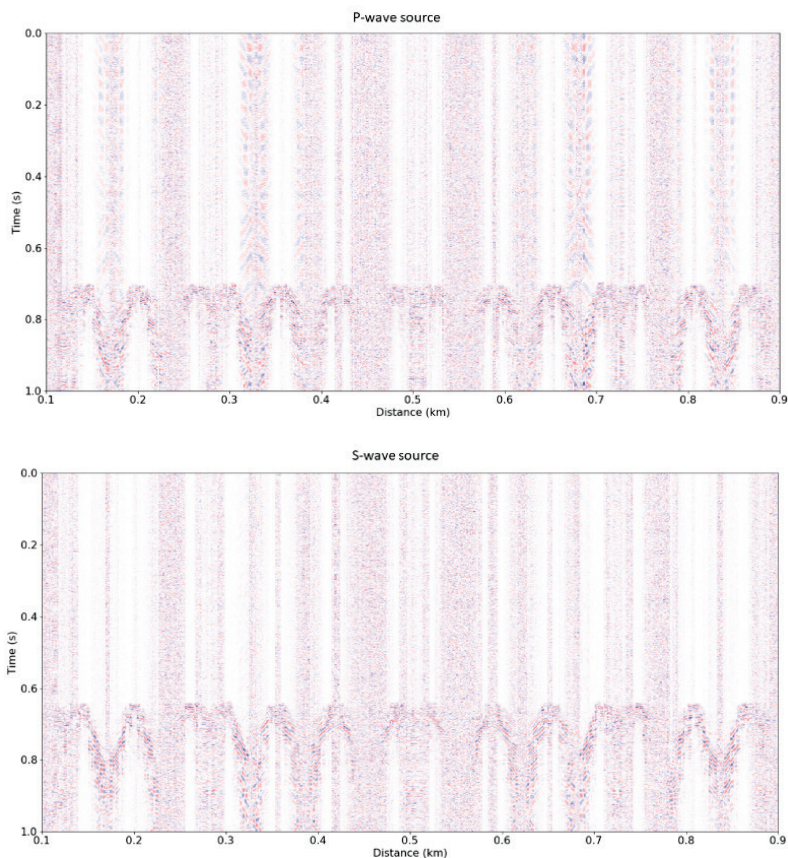


**Figure 15** DAS recording of a P-wave (above) and S-wave shot (below). Time 0.0 s is the shot time -10ms as provided by Uppsala University.

Large amplitude but low frequency noise is observed, particularly on the right-hand side of the dam which can be largely eliminated through bandpass filtering (e.g., Figure 16). There is also evidence that the base of the dam is highly attenuating as the active shots are recorded with low SNR on the cables at the base of the dam, both upstream and downstream (cables US1 and DS1, e.g., Figure 17).

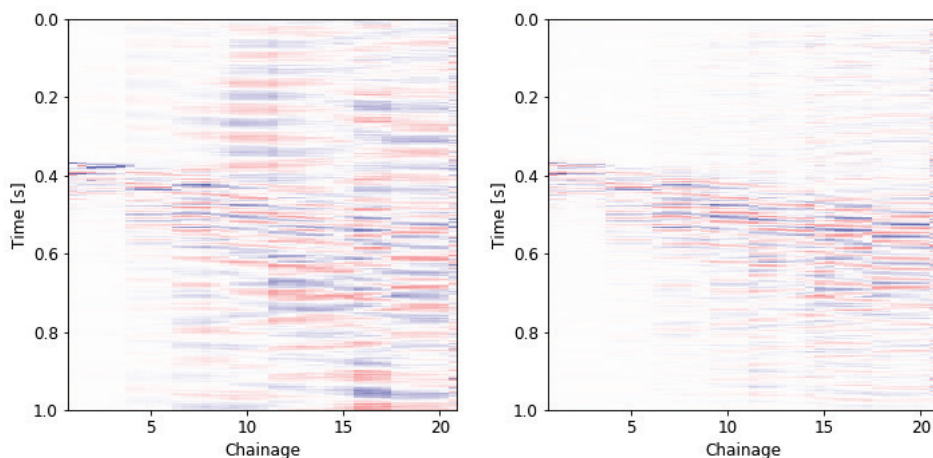


**Figure 16** Recording of an active shot on the crest cable (left) and the same data bandpass filtered between 20 and 250 Hz.

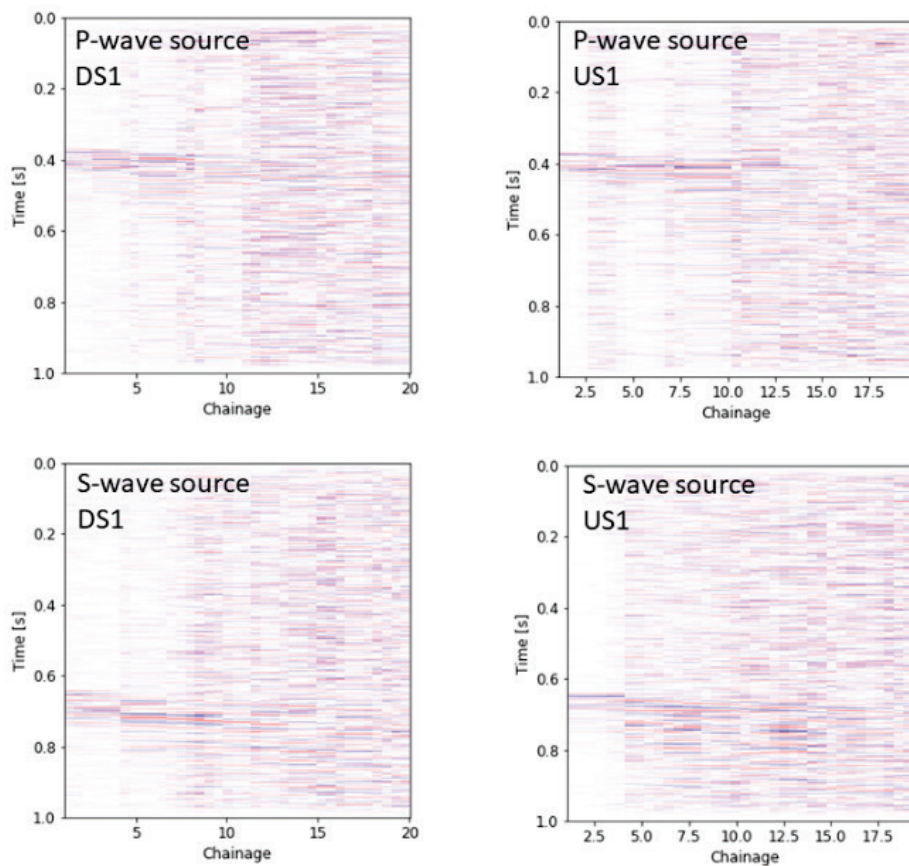


Figure 17 DAS shot recordings from the base of the dam on cables US1 and DS1. The data are bandpass filtered 20 – 250 Hz.

## 7 Results

### 7.1 IMAGING USING CREST CABLE

Eikonal tomography produced a velocity profile along the dam's core crest (see Figure 18a). The model obtained is well resolved between 1.5 m and 5.5 m depth. Velocities in the dam range between 160 to 320 m/s, and velocities below the dam range between 200 to 800 m/s. The velocity anomalies highlight the lateral variations (see Figure 18b) with strong positive and negative velocity variations up to 30% in the dam, and a strong positive velocity anomaly below the dam around Section 20.

The uncertainty in the model is the standard deviation computed from the 300 best fitting models (see Figure 18c). High uncertainties indicate that a wide range of  $V_s$  values fit the data. The misfit values represent how well best models fit data (see Figure 19). High misfit values indicate models that are outside the data error bars, although they can have low uncertainties.

As examples, Point #5 ( $X = 1\text{m}$ ) on Figure 10, has a low uncertainty together with a low misfit. This kind of points are reliable. They correspond to points in purple to blue on uncertainty and misfit plots. Point #14 shows high uncertainty and low misfit (Figure 20a). Point # 65 (see Figure 20b) shows a high misfit and low uncertainty. The model space could be extended here to allow models with a stronger decrease of velocity depth and higher velocity in the first layer. However, extending parameter range might lead to unrealistic models for other points. Here these high misfit values affect only few points. Local point #80 is an example of high misfit and high uncertainty (see Figure 20c). There, data error bar is difficult to fit all because of rapid velocity variations between periods.

Except for points around 16 metres, (Point #65), the final  $V_s$  model is thus reliable (Figure 18). The first 6 meters along dam's core crest show low velocities ( $< 180$  m/s) compared to the other part of the dam. This low velocity zone is cut by a sharp and narrow positive velocity anomaly at  $X = 3.25$  m (Point #14). Between  $X=6\text{m}$  and 20 m, velocities oscillate around 250 m/s with only one strong negative anomaly at about 18 m extending down to the dam bottom. The second layer of the model, along the dam bottom, shows a second low velocity anomaly at about  $X = 8$  m. Elsewhere, velocities oscillate around 230 m/s. Below the dam, velocities stay almost constant around 260 m/s, except at the far end of the dam ( $X > 18$  m), where they increase rapidly up to 800 m/s. Only one narrow negative velocity anomaly appears, just beneath the sharp positive anomaly in the dam at  $X = 3.25$  m.

Seismic velocity is related to material properties and velocity anomalies indicate variations in the material properties of the dam. Negative velocity anomalies at  $X = 8$  m and  $X = 18$  m most likely correspond to two weaker zones in the dam, such as high porosity/permeability zone and leaks (see Figure 18b). On the contrary, positive velocity anomalies at  $X = 3.25$  and  $X > 18\text{m}$  indicate tougher zones, with less elasticity, porosity and/or permeability. The overall trend of velocity increase from the top left edge to the bottom right of the dam could be related to material properties such as difference of compaction during the dam building, but also to

some boundary effects such as wave reflections on the surrounding walls enhanced by a strong noise directionality.

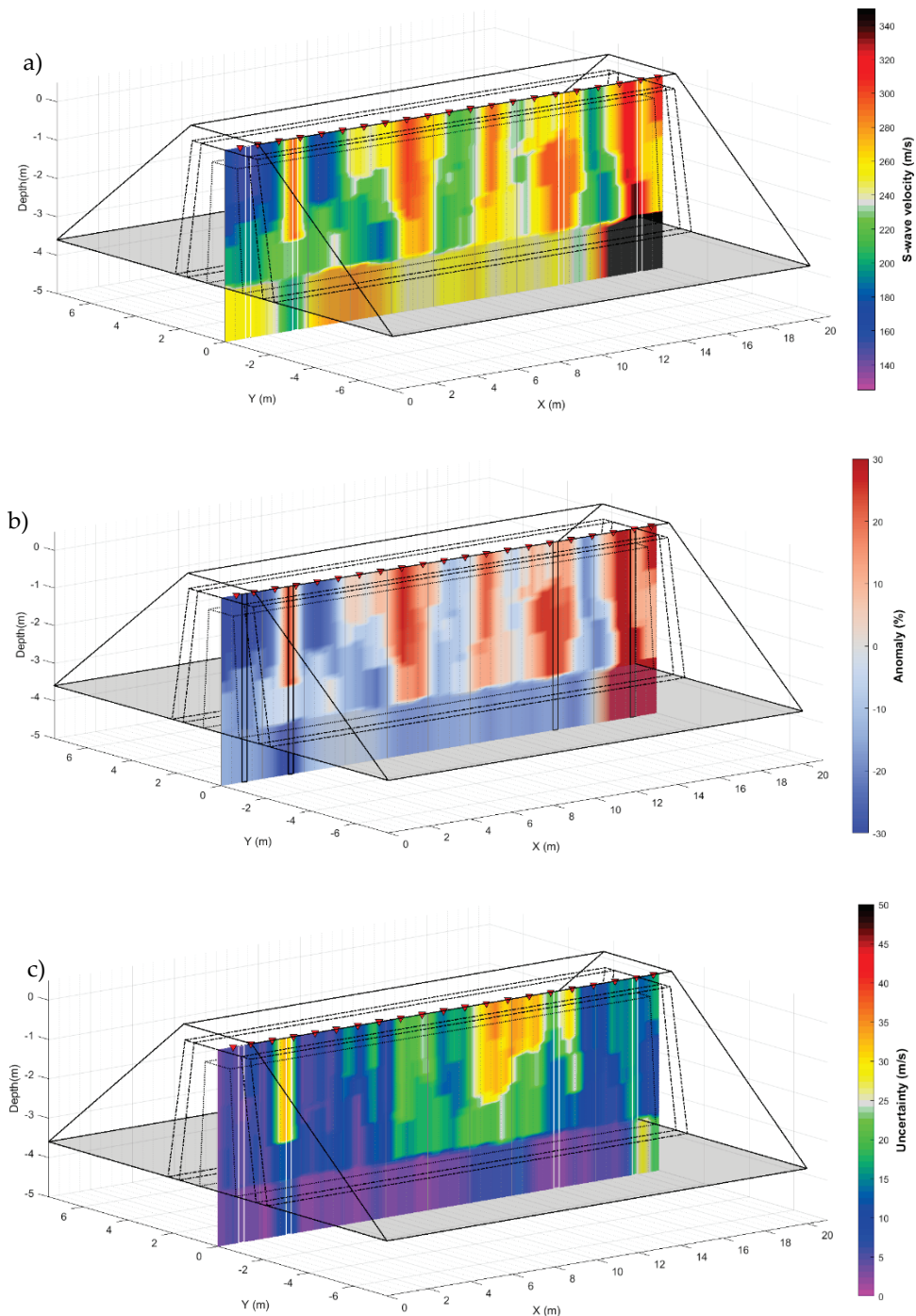


**Figure 18** Depth inversion results of dam's core crest tomography. Red triangles represent the channels used. a) S-wave velocity profile; b) Velocity anomaly profile; c) Velocity uncertainty profile. The X axis in metres correspond to the Section of the fibre in dam's core crest.

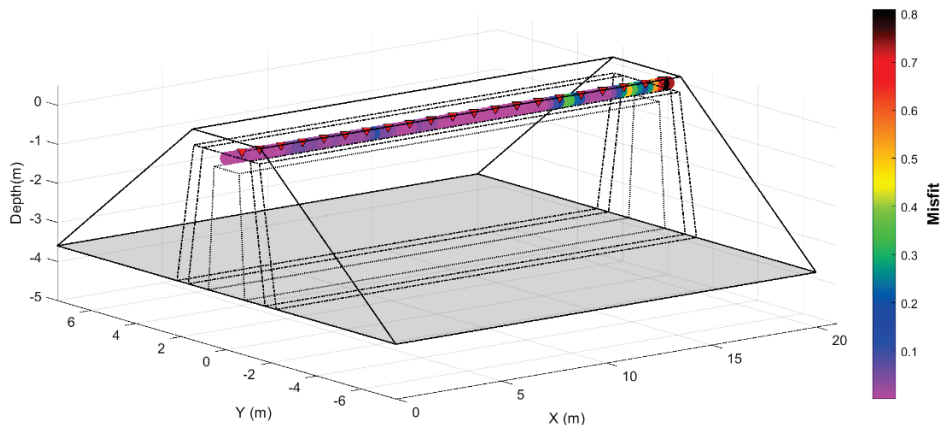


Figure 19 Misfit values along the core crest

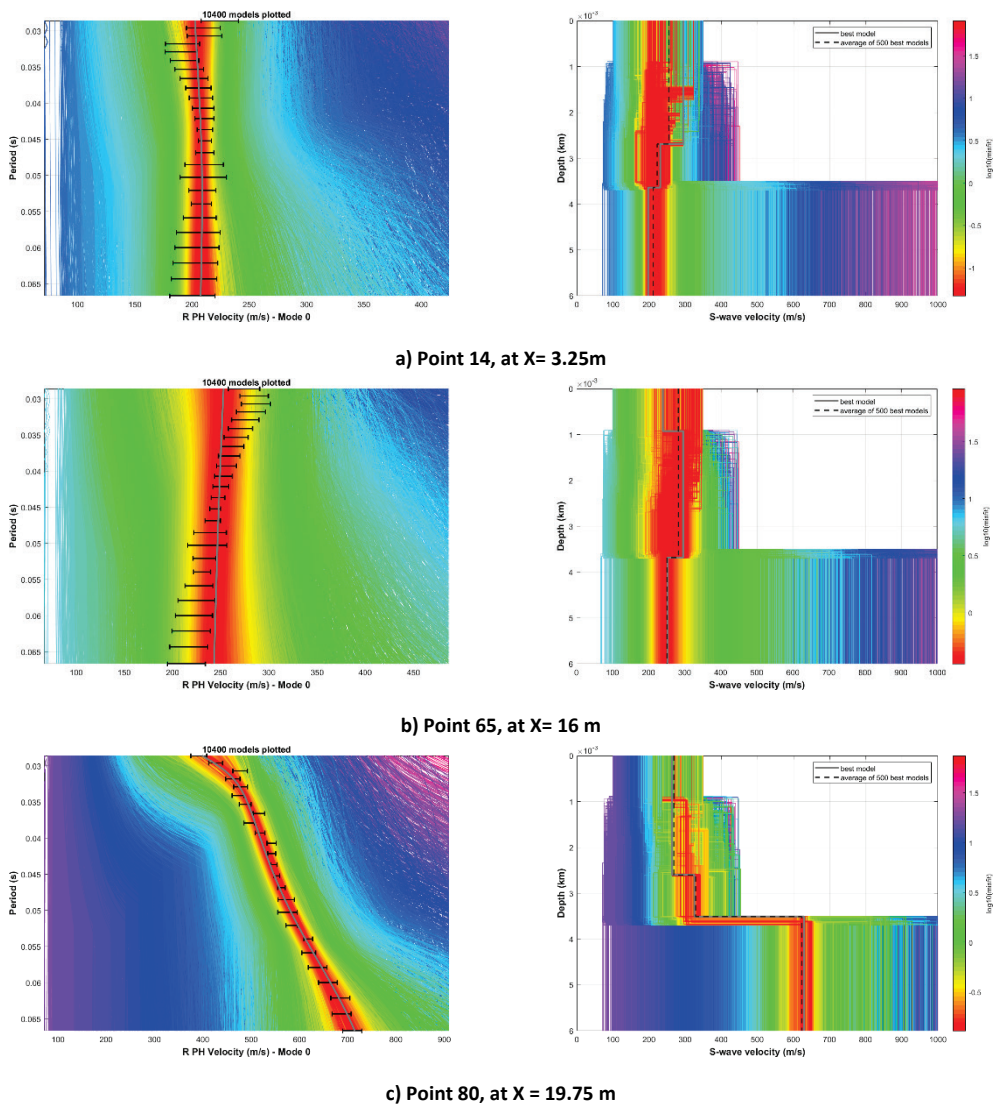


Figure 20 Example of local depth inversion for points discussed in the text. Locations of points is indicated on Figure 19.

## 7.2 PRELIMINARY INTER-CABLE IMAGING RESULTS

Stacking cross-correlations enhanced the arrival of a wave propagating inside the dam with a dominant of 20 Hz and an average velocity of about 250 m/s (white dotted line on Figure 21). This clear first arrival looks similar to the one measured at core crest. A second arrival appears to be a multiple of the first arrival with a travel-time four times longer (black dotted line on Figure 21).

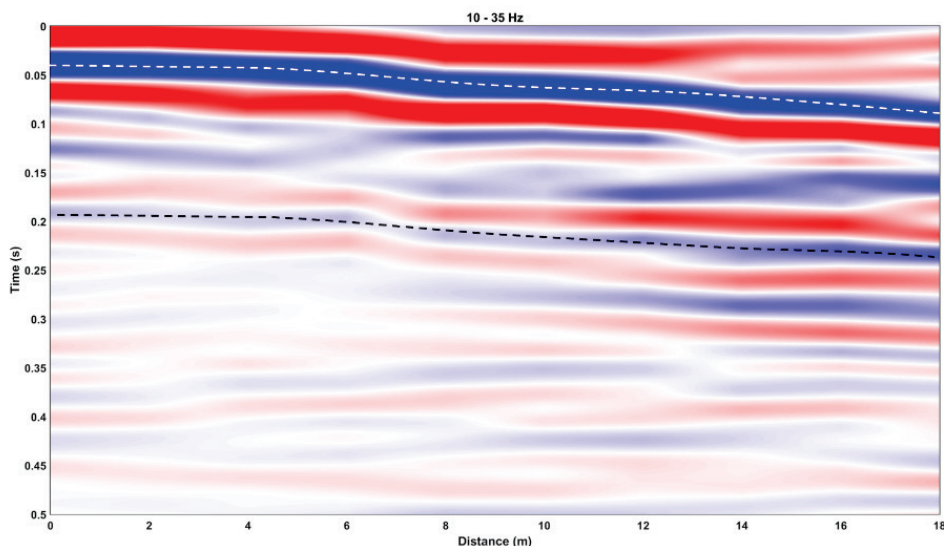
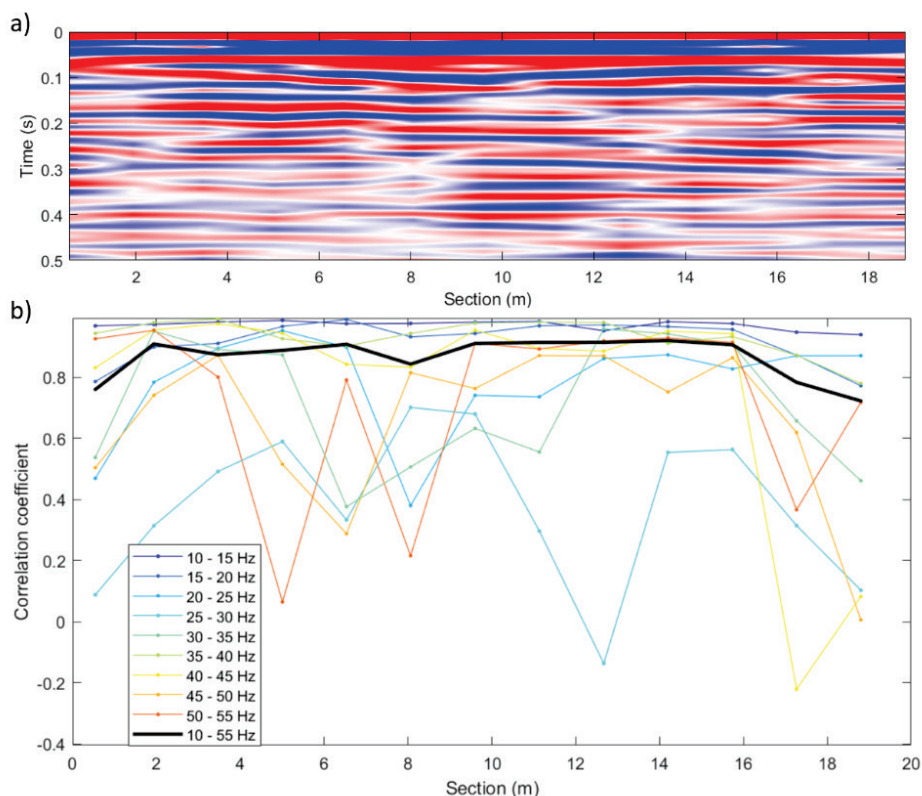


Figure 21 Stacked section of noise cross-correlations between USL2 et DSL3. Traces are bandpass filtered in between 10 and 35 Hz. White and black dotted lines highlight arrivals.

Correlation coefficients (CCF) reflects variation of velocities compared to average velocity of cross-correlations between facing channels of fibres USL2 and DSL3, i.e., on both side of dam's core. CCF were computed for a series of 5 Hz frequency bands and for a wide frequency band 10-55 Hz (this section is given in Figure 22a).

CCF for 10-55Hz shows velocity variations at both edges of the dam extending for 3.5m right-hand side of the dam and about 3 m on the left-hand side (black line on Figure 22b). A slight decrease in CCF is also visible at 8 m. All these velocity variations are coherent the velocity profile in Figure 18.

Taken individually, the lowest frequency bands are only sensitive to velocity variations at the dam's edges while the highest frequency waves are sensitive to velocity variations at Sections 5 m, 8m, and 17.3m. CCF for 30-35 Hz is low all along the dam with extreme low value 12.7 m. Intermediate frequency bands are sensitive to the velocity variations at 8 m



**Figure 22 a) Section used to compute average correlation for different frequency band (offset is constant, of about 2.1m). b) Correlation coefficient between average and individual correlations for different frequency band represented by colored lines. Thick black lines represent the correlation coefficient of data filtered between 10-55 Hz shown in a.**

### 7.3 MONITORING

Figure 23 shows travel time variations (black line) together with water temperature (red line) and water level measurements (blue line), for the whole recording duration for one channel pair (021.638.00-021.642.00). There is a significant travel-time decrease from the beginning of April until 23 April. The travel-time then stabilises until 5 May, when it starts to slowly increase. Measurements of water level and water temperature are available from this date. The travel-times displays consecutive step-like increases correlated with the refilling in water of the basin. These travel-time increase steps seem to have a greater amplitude each time there is a water replenishment. This exponential pattern of the travel time increase is also correlated with the long-term increase of the water temperature. The exponential increase of the travel time stops on 5 June. From this date, shorter trends of travel time variations are observed. A sharp decrease starts on 13 June with another rise several days later.

Daily oscillations of the travel times are observed all along the recording period. They seem to be slightly out of phase with the daily temperature variations.

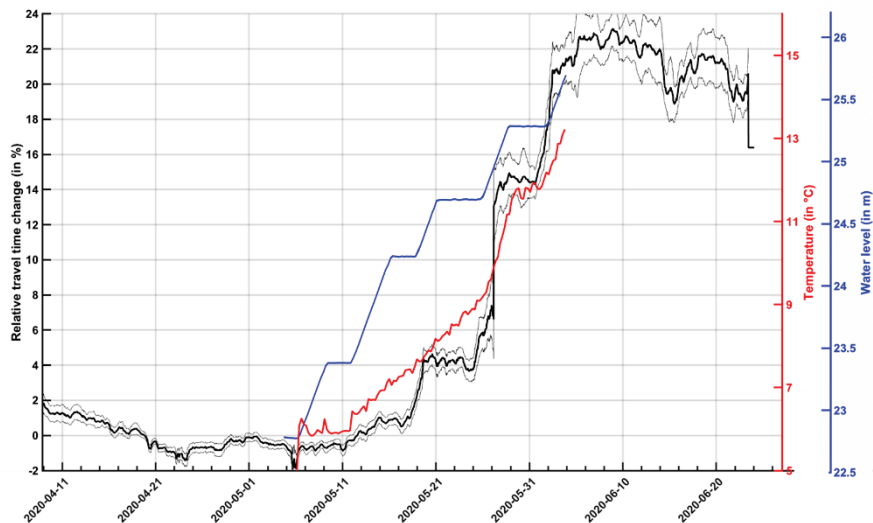


Figure 23 Example of relative travel-time changes as a function of time for the channel pair 021.638.00-021.642.00 (in black). The water level changes are represented in blue and the water temperature in red.

We analyse velocity variations ( $dv/v = -dt/t$ ) on each channel pair with a spacing of 2m, with 1 m overlaps. Figure 24 shows the velocity changes with time along the dam (centre panel), together with the average velocity variation over all pairs (top panel). Individual velocity changes are presented in the left panel for all channel pairs.

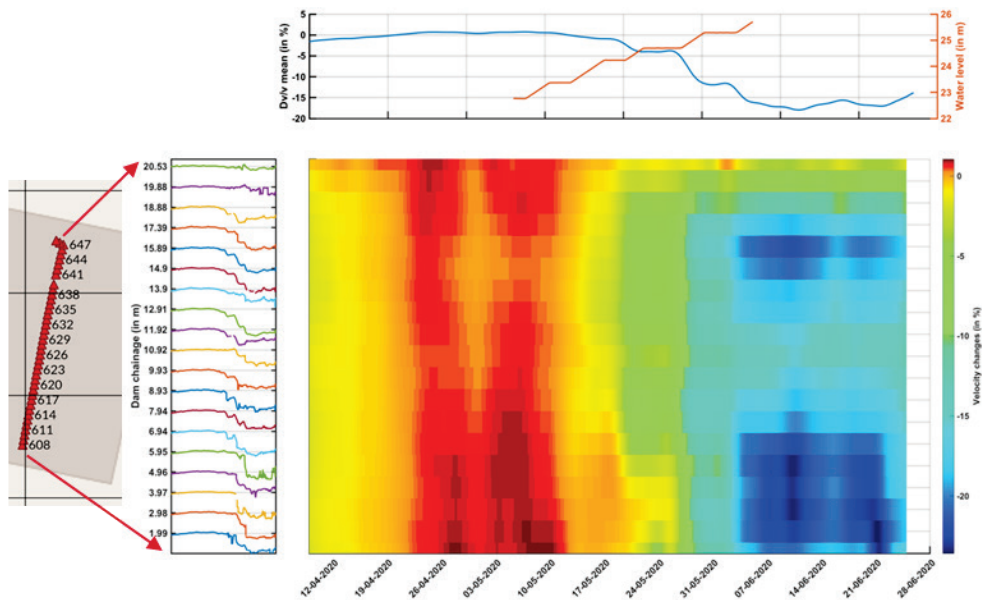


Figure 24 Relative velocity changes (in %) as function of time and dam chainage (center panel). Left panel shows velocity changes measurements for each pair of channels. Top panel represents the average velocity variations on all station pairs (in blue), together with water level variations (in red).

There is a small long-term increase in the average velocity on the order of 1% from the beginning of the monitoring period until the water level increase. Within this long-term pattern, a small decrease of velocity happens around 1 May with the most significant decreases between 8 m and 20m in dam chainage.

Between the first and second increases in water level (8 – 24 May), velocities start to decrease. Steps in velocity decrease are observed everywhere along the dam, with time delays of about one week of these fronts between 0 m and 8m and from >19.5 m.

Velocity changes are observed to be correlated with the first two rises in water level seem with a time delay. Velocity change steps are still correlated with later water levels rises and the velocity steps are large than those observed for the initial changes in water level.

Velocity changes start to vary laterally again after the final filling episode. Indeed, velocities vary by up to 24% from 0 m to 8 m and from 13 m to 19 m in dam chainage, but are less significant from 8 m to 13 m (about 8-10%). Finally, a significant short-lived peak of velocity increase occurs 14 – 15 June. The lateral variations in the velocity changes could be governed by the position of the water saturation front and the spatial variations of the permeability capacity of the dam.

Figure 25 represents the velocity change anomaly or residual, which is computed as the difference between each localized  $dv/v$  curves and the average  $dv/v$ . This representation of the results allows an improved identification of the spatial changes in velocities within the dam. As discussed above, the main lateral variations are observed after the water filling is completed, from 4 June. The second main lateral variation is observed 18 – 31 May, where the highest velocity drop is observed around 8 m in dam chainage and the highest velocity increase occurs 0 m to 7m in dam chainage. The delayed response between 0 m and 7 m dam chainage could indicate that a defect has been installed at a high level in the dam and it is therefore only recognisable with a high water level when there is a velocity decrease with increased water content.

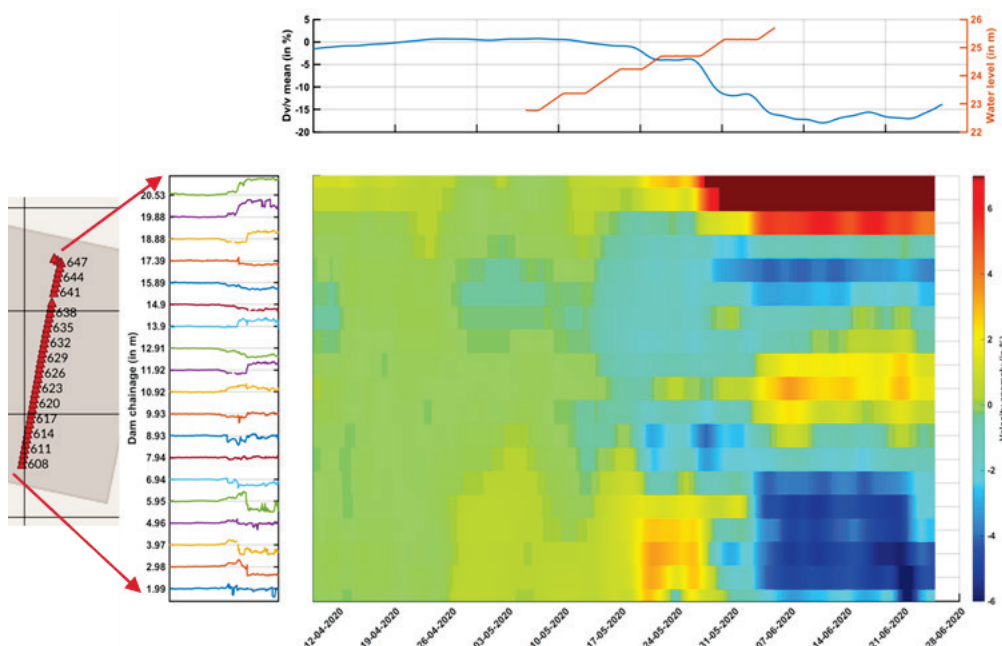


Figure 25 Velocity anomalies (in %) as function of time and dam chainage (center panel). Left panel shows velocity anomalies measurements for each pair of channels. Top panel represents the average velocity variations on all station pairs (in blue), together with water level variations (in red).

## 7.4 SUMMARY AND DISCUSSION

Velocity anomaly variations in time might result from changes within the structure of the dam, due to the defects that were added during construction. Indeed, the capacity of the dam to retain (or absorb) water will greatly affect the velocity of the surface waves within the dam as the water level rises. If that is the case, then the monitored velocity changes along time should also reflect the anomalies identified with the tomography of the dam.

Figure 26 shows the normalised velocity anomalies obtained with both the tomography and the monitoring approaches. While the tomography represents the spatial variations of surface wave velocities, the monitoring represents the evolution of the velocity variations in time along the dam. Negative anomalies are identified with blue circles while positive anomalies are highlighted with red circles. When comparing Figure 26a and b, a clear correlation of anomalies imaged and monitored from 0 m to 11m chainage appears. On 17 May, the water level rose up to 1m, hitting the bottom of the dam, where the tomography results indicate a positive anomaly and therefore possibly compacted, nonporous material (0 m – 6 m dam chainage; 3.5 m – 2.5 m deep). 17 – 25 May, monitoring results display positive anomalies in velocity changes at 0 m – 6 m dam chainage (negative and positive Anomaly 1 in Figure 26). After this period and until the end of the experiment, the anomalies become negative, possibly highlighting porous material and an increase in water saturation. This observation is in excellent accordance with the negative anomaly observed in the tomography.

Similar conclusions can be drawn for other parts of the dam. Results at 6-11 m and 18-20 m (negative and positive Anomalies 2, 3 and 4 in Figure 26) where there is good correlation between the tomography and monitoring results and could be interpreted as porous, high-water content material for the blue anomalies and non-porous impermeable material for positive anomalies. Slight discrepancies probably only result from the different resolutions obtained with each of the two methods.

It is possible track the waterfront evolution along the dam as a function of time for chainage 0-11 m and 18-20 m.

There is however no correlation between the tomography and monitoring results for dam chainage 11-18m, possibly reflecting more complex physical processes.

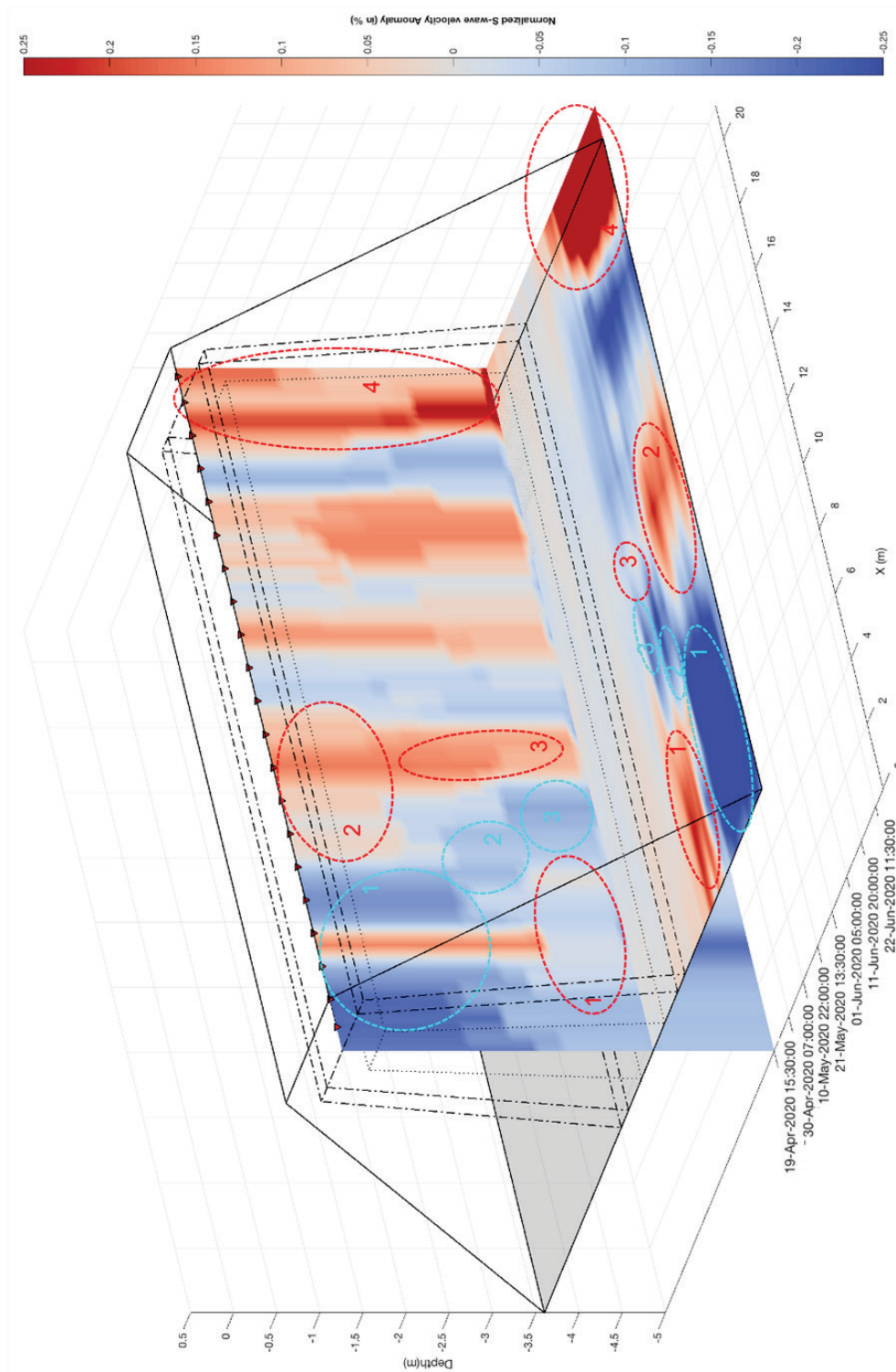


Figure 26 Summary figure of the passive seismic survey along the test dam. Anomalies are normalized to enable easier comparison of the imaging and monitoring results. Note, water filling began on 7 May.

## 8 Conclusions and Recommendations

### 8.1 CONCLUSIONS

Fibre-optic monitoring at the Test Dam with a DAS interrogator with a 3 m gauge length provided high-quality data suitable for ambient noise interferometry analysis. This data has been used to

- Perform measurements during water filling to detect changes seismic velocity that could be caused by changes in material properties in the dam.
- Improve the spatial resolution compared to previous combined DAS-ANI measurements with a 3 m gauge length instrument.
- Demonstrate that available ANI methods can be applied at such small-scale dams to image and monitor the infrastructure.

Ambient noise imaging using the dam's core crest cable revealed strong lateral velocity variations along the dam. Despite some strong misfits or uncertainties, the velocity model is reliable between 1.5 and 5.0 m deep. It shows strong, wide, opposite velocity anomalies at each of the dam's extremities. It also shows negative anomalies at 8 m and 18 m that could correspond to weakening defects and /or leaks, while at 3.25 m the strong positive anomaly could indicate a strengthening effect.

Attempts to use inter-fibre cross-correlations for imaging show very encouraging results. The propagating waves recorded are similar those used from the dam's core crest. A stacked section even shows a multiple arrival. A negative anomaly at 8 m and velocity changes at the dam's extremities were also found from a simple correlation coefficient analysis. This coherence of results reinforces the reliability of the velocity profile but also encourages further developments of 3D imaging using several fibre sections in different part of the dam.

The monitoring analysis reveals a clear anti-correlation of the velocity variations and water filling, suggesting a sensitivity of the seismic waves to water content in and/or around the dam. There is also a clear anti-correlation of the velocity variations with temperature measurements on a long-term basis. On a shorter-term basis, velocity variations are slightly out of phase with the daily temperature variations. Velocity variations anomalies observed at different places in the dam over time could potentially track saturation effects and the waterfront rising in the dam.

A joint analysis of both imaging and monitoring results reveals a correlation of the observed anomalies in space and time at several places in the dam and confirms that both techniques could be used jointly for monitoring water seepage along the dam. The delayed time response of the dam to the water filling as seen from the monitoring clearly indicates heterogeneities within the dam and differences in the response along the dam at a given height may highlight different effective permeabilities within the dam.

Simulations of these results would help explain the discrepancies observed between the different methods in some parts of the dam.

Active P- and S-wave shots on the dam were well recorded by the DAS interrogator but unknown absolute source timings do not allow for a standard analysis. Further analysis is required to determine relative timings.

## 8.2 EXTENSION OF THE ANALYSIS

The DAS-ANI analysis has provided significant results that could be investigated further with additional analysis.

- With the use of several different upstream and downstream fibre section 3D imaging should be possible.
- The velocity changes could be modelled to determine the effect of environmental and hydrogeological parameters on absolute shear-wave velocities and therefore more accurately assess temporal variations in the dam.
- A time-lapse tomographic model could be used to determine velocity changes in the dam and verify consistency with the monitoring results. This would only be possible where significant changes (greater than a few %) are observed.
- Simulations of these results would help explain the discrepancies observed between the imaging and monitoring results observed in some parts of the dam.
- An analysis of the active shot data could be conducted through the correlation of shot recordings.

## 9 References

- RIDAS (2019). Kraftföretagens riktlinjer för dammsäkerhet, Swedenergy AB.
- Becker, M. W., & Coleman, T. I. (2019). Distributed Acoustic Sensing of Strain at Earth Tide Frequencies. *Sensors*, 19(9), 1975. doi: 10.3390/s19091975.
- Biot, M.A., 1956. Theory of elastic waves in a fluid-saturated porous solid. 1. Low frequency range. *Journal of the Acoustic Society of America* 28, 168-178.
- Boleve A., Vandermeulebrouck J. & Grangeon J. (2012) Dyke leakage localization and hydraulic permeability estimation through self-potential and hydro-acoustic measurements: Self-potential 'abacus' diagram for hydraulic permeability estimation and uncertainty computation, *Journal of Applied Geophysics*, 86, 17-28.
- Buck C.J. & Watters, R.J. (1986) Acoustic emission generation from water flow through granular soils, *Proc., 22nd Symp. on Engineering Geology and Soils Engineering*, Boise, Id., 138–154.
- Curtis, A., Gerstoft, P., Sato, H., Snieder, R., Wapenaar, K., 2006. Seismic interferometry turning noise into signal. *Leading Edge* 25, 1082–1092.
- de Ridder, S. A. L., B. L. Biondi, and R. G. Clapp (2014). Time-lapse seismic noise correlation tomography at Valhall, *Geophys. Res. Lett.*, 41, 6116–6122, doi:10.1002/2014GL061156.
- Foster M., Fell R. & Spannagle M. (2000) The statistics of embankment dam failures and accidents. *Canadian Geotechnical Journal* 37: 1000-1024.
- Fell R., MacGregor P., Stapledon D. & Bell G. (2005) *Geotechnical engineering of embankment dams*, A.A. Balkema, ISBN: 04-1536-440-x, 912p.
- Gassmann, F., 1951. Über die Elastizität poröser Medien. *Veierteljahrsschrift der Naturforschenden Gesellschaft in Zurich* 96, 1-23.
- Huang, Y., Ohkura, T., Kagiya, T., Shin Yoshikawa & Hiroyuki Inoue (2018). Shallow volcanic reservoirs and pathways beneath Aso caldera revealed using ambient seismic noise tomography. *Earth Planets Space*, 70, 169, doi:10.1186/s40623-018-0941-2.
- ICOLD (2015), Internal erosion of existing dams, levees and dikes, and their foundations, *Bulletin 164 Volume 1: Internal erosion processes and engineering assessment*, ICOLD Bulletin 164, 156p.
- Jousset, P., Reinsch, T., Ryberg, T., Blanck, H., Clarke, A., Aghayev, R., ... Krawczyk, C. M. (2018). Dynamic strain determination using fibre-optic cables allows imaging of seismological and structural features. *Nature Communications*, 9(1). doi: 10.1038/s41467-018-04860-y.
- Johansson, S. (1997) *Seepage monitoring in embankment dams*. Doctoral Thesis, TRITA-AMI PHD 1014, ISBN 91-7170-792-1, Royal Institute of Technology, Stockholm.
- Johansson, S. and Nilsson, Å. (2005). Internal Erosion Detection at the Røsvatn Test Site - Experiences from blind test using Resistivity, Self-Potential, Temperature, and Visual inspection. Part A – Assessment report. *Elforsk rapport 05:42*, Stockholm.
- Johansson S., Stork A., David A., Mondanos M., and Nygren C. 2020. Fibre-optic Distributed Acoustic Sensing for detection of seepage and internal erosion, *Energiforsk*, Report 2020:682, ISBN 978-91-7673-682-1.
- Johansson et al., in prep, ICOLD Congress
- Koerner R.M., McCabe W.M. & Baldivieso L.F. (1981) Acoustic emission monitoring of seepage, *J. Geotech. Engrg. Div.*, 107 4, 521–526.
- Koerner R.M., Reif J.S. & Burlingame M.J. (1979) Detection methods for location of subsurface water and seepage, *J. Geotech. Engrg. Div.*, 105 11, 1301–1316.

- Koerner R.M., Lord A.E., Jr. & McCabe, W.M. (1976) Acoustic emission Microseismic monitoring of earth dams, Proc., Conf. on Evaluation of Dam Safety, Pacific Grove, ASCE, New York, 274–291.
- Lin, F.-C., Ritzwoller, M.H., Townend, J., Bannister, S., Savage, M.K., 2007. Ambient noise Rayleigh wave tomography of New Zealand. *Geophys. J. Int.* 170, 649–666. doi: 10.1111/j.1365-246X.2007.03414.x.
- Lindsey N. J., Martin, E. R., Dreger, D. S., Freifeld, B., Cole, S., James, S. R., Biondi, B.L. & Ajo-Franklin, J. B. (2017). Fibre-optic network observations of earthquake wavefields. *Geophysical Research Letters*, 44, 11, 792–11,799. doi:10.1002/2017GL075722.
- Nikles, M. (2009). Long-distance fibre optic sensing solutions for pipeline leakage, intrusion, and ground movement detection. *Fibre Optic Sensors and Applications VI*. doi: 10.1117/12.818021.
- Olivier, G., F. Brenguier, T. de Wit and R. Lynch (2019). Monitoring the stability of tailing dam walls with ambient seismic noise, *The Leading Edge*, 36(4), 72 – 77.
- Parker, T., Shatalin, S., & Farhadiroushan, M. (2014). Distributed Acoustic Sensing – a new tool for seismic applications. *First Break*, 32(2010). doi: 10.3997/1365-2397.2013034.
- Planès, T., Mooney, M. A., Rittgers, J. B. R., Parekh, M. L., Behm, M., & Snieder, R. (2016). Time-lapse monitoring of internal erosion in earthen dams and levees using ambient seismic noise. *Géotechnique*, 66(4), 301–312. doi: 10.1680/jgeot.14. p.268.
- Shapiro, N.M., Campillo, M., Stehly, L., Ritzwoller, M.H., 2005. High-resolution surfacewave tomography from ambient seismic noise. *Science* 307, 1615–1618.
- Sjödahl, P., Dahlin, T., Johansson, S. (2019). Geofysiska metoder inom dammsäkerhetsområdet. *Energiforsk rapport 2019:571* ISBN 978-91-7673-571-8.

Precipitation data, retrieved February 14, 2020, from:

<http://www.smhi.se/data/meteorologi/ladda-ner-meteorologiska-observationer/#param=precipitation24HourSumstations=all,stationid=106040>

Air temperature data, retrieved February 14, 2020, from:

<http://www.smhi.se/data/meteorologi/ladda-ner-meteorologiska-observationer/#param=airtemperatureMean24h,stations=all,stationid=106040>



# DISTRIBUTED ACOUSTIC SENSING FOR DETECTION OF DEFECTS IN THE TEST DAM AT ÄLVKARLEBY

Optiska fibrer för att mäta läckage eller rörelse finns i nästan 100 dammar i Sverige idag. Det betyder att man kan få fram seismiska gånghastigheter och information när materialets egenskaper avviker från det normala.

Genom att mäta temperaturen kan läckage detekteras och genom töjningsmätning kan man upptäcka om materialet rör sig. Flertalet installationer kan också användas för akustisk mätning, så kallad Distributed Acoustic Sensing, DAS. Utvecklingen av DAS har gått snabbt framåt de senaste åren.

Här redovisas resultat från Vattenfalls testdamm i Älvkarleby som visar att seismiska gånghastigheter kan fastställas och extraheras och ge information om avvikande materialegenskaper. Om det här överensstämmer med inbyggda defekter kommer att bedömas när läget för de olika defekterna presenteras.

Energiforsk is the Swedish Energy Research Centre – an industrially owned body dedicated to meeting the common energy challenges faced by industries, authorities and society. Our vision is to be hub of Swedish energy research and our mission is to make the world of energy smarter!